2. Materials and methods

2.1. Materials

CPT-11 was a kindly gift from Yakult Co., Ltd. (Tokyo, Japan). Distearoylphosphatidylcholine (DSPC) and methoxy-poly(ethyleneglycol)-distearylphosphatidylethanolamine (PEG-DSPE, PEG mean molecular weight, 2000) were purchased from the NOF Corporation (Tokyo, Japan). SN-38 and cholesterol (Ch) were purchased from Wako Pure Chemical Industries, Ltd. (Osaka, Japan). IP-6 solution was obtained from Nacalai Tesque Inc. (Kyoto, Japan). RPMI-1640 medium and fetal bovine serum (FBS) were obtained from Invitrogen Corp. (Carlsbad, CA, USA). Other reagents were of analytical or HPLC grade.

2.2. Preparation of liposomal CPT-11

Liposomes were prepared by a modified ethanol injection method [23]. Briefly, DSPC, Ch and PEG-DSPE at a molar ratio of 55:45:5 (40 mg/16 mg/12.5 mg) were dissolved in ethanol. Ethanol was removed by rotary evaporation at 70 °C to a smaller volume until one-tenth of the volume of hydration buffers. To prepare liposomal IP-6, liposomal Cu and liposomal Cit, 1.5 mL of 100 mM IP-6 solution adjusted to pH 6.5 using triethanolamine (TEA), 300 mM $CuSO_4$ solution adjusted to pH 3.4 with H_2SO_4, and 500 mM citrate buffer adjusted to pH 3.0 with HCl were used as hydration buffer, respectively. Hydration buffer was added to the lipid-ethanol solution immediately, followed by extensive vortex mixing and sonication at 70 °C. Liposomal IP-6 and Cu were treated with 5 circles of freezing (−80 °C) and thawing (60 °C), and extraliposomal buffer was exchanged for SHE-buffer (300 mM sucrose, 20 mM HEPES and 15 mM EDTA, pH 7.4) by size exclusion chromatography on a Sephadex G-50 column. In liposomal Cit, extraliposomal pH was adjusted to 7.4 with NaOH before CPT-11 loading according to the pH gradient method [9]. The particle size distribution was measured by ELS-Z2 (Otsuka Electronics Co., Ltd., Osaka, Japan) at 25 °C after diluting the dispersion to an appropriate volume with water.

CPT-11 was added to liposomal IP-6, Cu and Cit at a desired CPT-11-to-DSPC weight ratio of 0.2 to 2.0 (equivalent to CPT-11-to-total lipid of 0.12 to 1.2), and incubated at 60 °C for 1 h for drug loading, and then quenched on ice for 5 min. Here, liposomal CPT-11 prepared by the pH gradient method with citrate buffer, and Cu- and IP-6-mediated methods were named as Cit-, Cu- and IP6-L, respectively. Unencapsulated CPT-11 was removed using a Sephadex G-50 column eluted with saline adjusted to pH 7.4. CPT-11 concentration was determined using a fluorometer (Wallac ARVO SX1420 multi-label counter, PerkinElmer Japan, ex: 375 nm, em: 535 nm) in a solubilized sample after the addition of an equal volume of cold acid methanol (5 mM HCl in methanol), and then the loading efficiencies of CPT-11 in the liposomes were calculated. The concentration of phospholipid (DSPC) was measured with the Phospholipids C-test Wako (Wako Pure Chemical Industries, Ltd.). IP-6 concentration in the liposome was determined by inductively coupled plasma (ICP) analysis (SPS7800, SII Nano Technology Inc., Tokyo, Japan). Briefly, the phosphorus concentration of IP-6 in IP6-L was calculated by subtracting the phosphorus concentration of empty liposomes from that of IP6-L.

2.3. Pharmacokinetic analysis

CPT-11 in saline and IP6-, Cu- and Cit-L were used for in vivo studies. Female ddY mice (5 weeks old; Sankyo Lab Service Corp., Tokyo, Japan) were injected with a single intravenous bolus via the lateral tail vein at a dose of 10 mg/kg. At 1, 6, 24 and 48 h after injection, blood was collected using a heparinized syringe and centrifuged to obtain plasma at 1500 g for 30 min. CPT-11 and SN-38 in plasma were extracted with the addition of an equal volume of cold acidic methanol. The mixture was vortexed for 10 s and incubated at −80 °C for more than 5 h until analysis. After thawing, the samples were centrifuged at 100,000 g for 30 min at 4 °C by ultracentrifugation (CS120 GXL, Hitachi, Japan) to remove aggregated protein. The supernatant was applied to a TSKgel ODS-80Ts QA 5 μm column (4.6 mm I.D.×25 cm, Tosoh, Co., Ltd., Tokyo, Japan) equilibrated in 75 mM ammonium acetate, 35% acetonitrile, pH 4.0, at a flow rate of 1 mL/min. CPT-11 and SN-38 were detected with an HPLC system (Shimadzu Co.) composed of an LC-10AS pump, an SIL-10A autoinjector and an RF-10A_{XL} fluorescence detector using an excitation wavelength of 375 nm and an emission wavelength of 530 nm. Under these conditions, CPT-11 and SN-38 were eluted at 4.7 min and 7.2 min, respectively. The CPT-11 dose%/mL plasma and dose% /g tissue were calculated by dividing the amount of CPT-11 per total plasma volume (mL) and per total tissue weigh (g), respectively, by that of the injected liposomal CPT-11. The total volume of plasma was calculated using the reported volume of mouse plasma, 48.8 mL/kg [24]. Pharmacokinetic parameters were calculated using the bootstrap method [25], including the plasma area under the curve (AUC) from 1 to 48 h, clearance (CL), mean residence time (MRT) and half life period ($T_{1/2}$).

2.4. Drug sensitivity in vitro

Murine colon carcinoma Colon 26 cells were obtained from the Cell Resource Center for Biomedical Research, Tohoku University (Miyagi, Japan). Human colorectal adenocarcinoma COLO 320DM cells were purchased from the American Type Culture Collection (Manassas, VA, USA). The cells were cultured in RPMI-1640 medium with 10% heat-inactivated FBS and 100 μg/mL kanamycin sulfate in a humidified atmosphere containing 5% CO_2 at 37 °C.

Colon 26 cells were seeded separately at a density of 1×10^3 cells per well in 96-well plates and maintained for 24 h before treatment in RPMI-1640 medium supplemented with 10% FBS. To examine cytotoxicity for IP-6, the cells were treated with medium containing from 0.0625 to 1 mM IP-6. For combination therapy, the cells were treated with medium containing various concentrations of CPT-11, ranging from 0.625 to 10 μM, or SN-38, ranging from 0.625 to 10 nM, in the presence or absence of 0.1 mM IP-6. The cells were incubated for 72 h. The cell number was determined with a cell counting kit (Dojindo Laboratories, Kumamoto, Japan). Cell viability was expressed relative to the absorbance at 450 nm of untreated cells.

2.5. CPT-11 biodistribution in Colon 26 tumor

To generate Colon 26 tumor, 1×10^6 cells suspended in 100 μL of RPMI medium were inoculated subcutaneously into the flank of female CDF1 mice (5 weeks of age; Sankyo Labo Service Corporation, Tokyo, Japan). The tumor volume was calculated using the formula; tumor volume $= 0.5\times a\times b^2$, where a and b are the larger and smaller

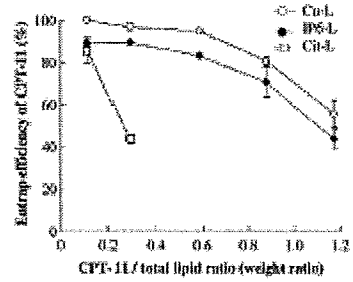

Fig. 1. The effect of the drug-to-lipid weight ratio on CPT-11 loading to liposomal Cit, Cu and IP-6 incubated at 60 °C for 1 h. The extent of CPT-11 encapsulation was determined. Each result represents the mean ± S.D. ($n = 3$).

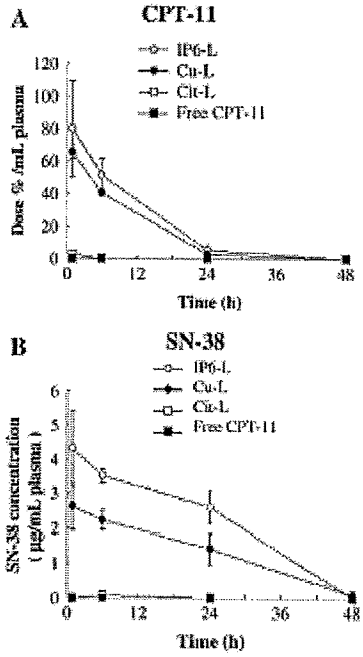

Fig. 2. Plasma CPT-11 dose% (A) and SN-38 concentration (B) in mice following a single intravenous injection dose of liposomal CPT-11 (equivalent to 10 mg CPT-11/kg) in ddY mice. The plasma concentration was determined as a function of a time. Data points represent the mean CPT-11 dose% (A) and SN-38 concentration (B) ± SD ($n = 3$).

diameters, respectively. When the average volume of the tumors reached 100–150 mm^3, CPT-11 solution and IP6-, Cu- and Cit-L were intravenously administered *via* lateral tail veins at a dose of 10 mg CPT-11/kg (24.7 mg lipid/kg). Twenty-four hours after injection, blood was collected with a heparinized syringe and centrifuged to obtain plasma. The tumor, liver, spleen, kidney and lung were excised and homogenized in phosphate-buffered saline (pH 7.4). CPT-11 and SN-38 were extracted with cold acid methanol and analyzed by the HPLC system as described above.

2.6. Therapeutic study

To generate COLO 320DM tumor xenografts, 1×10^7 cells suspended in 100 μl of RPMI-1640 medium were inoculated subcutaneously into the flank of female BALB/c nu/nu mice (5 weeks of age; CLEA Japan, Inc., Tokyo, Japan). Colon 26 tumors were generated as described above. When the average volume of Colon 26 tumor and COLO 320DM tumor xenografts reached 50–100 mm^3 (day 1), CPT-11 solution, and IP6- and Cu-L were injected (10, 20 or 60 mg/kg) into a tail vein at once or in three injections at three-day intervals. IP6-L administered at 20 mg CPT-11/kg resulted in co-administration of IP-6 at 36 mg/kg. IP6-L was concentrated with Amicon Ultra centrifugal filter devices (Millipore, MA, USA) when injected at 60 mg/kg. Tumor volume and body weights were measured for individual animals. Animal experiments were performed with approval from the Institutional Animal Care and Use Committee at Hoshi University.

2.7. Statistical analysis

The statistical significance of differences between mean values was determined using Welch's *t* test. Multiple comparisons were evaluated by analysis of variance (ANOVA) with Tukey's multiple comparison test. *P*-values less than 0.05 were considered significant.

3. Results

3.1. Preparation of liposomal CPT-11

IP-6 was used for the proposed novel loading process of CPT-11 in liposomes as an intraliposomal trapping agent to improve encapsulation efficiency and tumor toxicity. Liposomal IP-6 was prepared using 100 mM IP-6 solution adjusted with TEA to pH 6.5, in which total lipid concentration was 14.6 mg/mL. For comparison with traditional loading methods of CPT-11, we prepared liposomal Cu for the ion chelating method [10], and liposomal Cit for the pH gradient method [9]. In all cases, the average particle diameter of each liposome was approximately 100–150 nm with a narrow, monodisperse distribution (less than 0.2 in polydispersity index). After loading CPT-11 into the liposomes, all liposomal CPT-11 were approximately 150 nm in size (data not shown). IP6- and Cu-L at CPT-11 to total lipid ratios from 0.12 to 0.6 exhibited 90–100% loading efficiency (Fig. 1). In contrast, Cit-L showed only 40% loading efficiency at a CPT-11 to total lipid ratio of 0.3. At least two weeks after preparation, encapsulated CPT-11 in IP6-L was stable and did not release CPT-11 (data not shown). For this reason, in subsequent experiments, we prepared IP6-, Cu- and Cit-L at CPT-11 to total lipid weight ratios of 0.6, 0.6 and 0.12, respectively. The final CPT-11 concentration was 0.5–0.8 mg/mL, and drug-to-IP-6 (mol/mol) in IP6-L was 0.54.

3.2. Plasma CPT-11 and SN-38 levels in mice after intravenous injection of liposomal CPT-11

To investigate the stability of liposome *in vivo*, plasma dose% and concentrations of CPT-11 and SN-38 were shown in Fig. 2 and the pharmacokinetic parameters of IP6- Cit- and Cu-L were calculated (Table 1). After administration of free CPT-11 and Cit-L, CPT-11 was eliminated rapidly from plasma, and SN-38 had almost disappeared from plasma 24 h after injection. In contrast, IP6- and Cu-L maintained higher CPT-11 and SN-38 levels throughout 24 h (Fig. 2A and B). The AUC of CPT-11 in Cu- and IP6-L (1477.16 and 1929.35 μg h mL^{-1}) was 62- and 81-fold higher than that of Cit-L (23.83 μg h mL^{-1}), respectively. These trends were also observed in SN-38. Clearances of CPT-11 in IP6- and Cu-L were greatly reduced, but that of Cit-L was faster than those of IP6- and Cu-L, indicating that CPT-11 in Cit-L leaked rapidly from liposomes. MRT and $T_{1/2}$ for CPT-11 in Cu-L and IP6-L were longer than those in Cit-L. IP6-, Cu- and Cit-L had the

Table 1
The calculated CPT-11 and SN-38 pharmacokinetic parameters following a single i.v. dose of liposomal CPT-11

Liposome	CPT-11				SN-38	
	$AUC_{0-\infty,n}$ (μg h mL^{-1})	CL (L h^{-1} kg^{-1})	MRT (h)	$T_{1/2}$ (h)	$AUC_{0-\infty,S}$ (μg h mL^{-1})	MRT (h)
Cit-L	23.83 ± 1.93	0.42 ± 0.04	4.2 ± 0.33	2.9	1.20 ± 0.11	9.79 ± 0.98
Cu-L	1477.16 ± 50.77 *	0.01 ± 0.00	6.20 ± 0.37	4.3	64.63 ± 8.23 *	14.40 ± 1.28
IP6-L	1929.35 ± 241.75 *	0.01 ± 0.00	6.82 ± 0.55	4.8	108.34 ± 9.10 *	14.55 ± 0.85

AUC: area under the curve, CL: clearance, MRT: mean residence time, $T_{1/2}$: half-life period. * $P < 0.05$ ddY mice were given a single i.v. bolus dose equivalent to 10 mg CPT-11/kg.

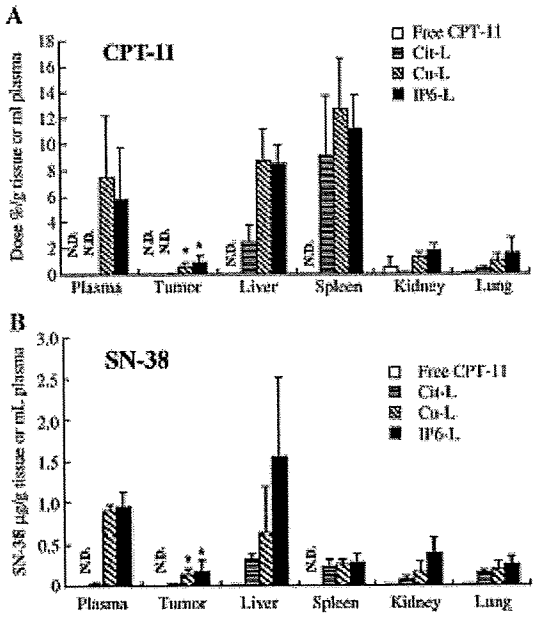

Fig. 3. Biodistribution of liposomal CPT-11 at 24 h after single injection in mice bearing Colon 26 tumor. Tissue and tumor biodistribution of CPT-11 (A) and SN-38 (B) after single intravenous injection doses (equivalent to 10 mg CPT-11/kg) of free CPT-11, Cit-L, Cu-L and IP6-L. Each value represents the mean ± S.D. ($n=3$). *$P<0.05$, compared with free CPT-11. N.D.: not detected.

same lipid formulation, but the pharmacokinetic parameters were completely different. These results indicated that liposomal formulations with intraliposomal drug-trapping agents improved CPT-11 retention in blood following intravenous injection.

3.3. CPT-11 and SN-38 biodistribution in Colon 26 tumor

The biodistribution profiles of liposomal CPT-11 and free CPT-11 were determined 24 h after intravenous injection of 10 mg CPT-11/kg into mice bearing Colon 26 tumor (Fig. 3A and B). After injection of free CPT-11, CPT-11 and SN-38 concentrations in tissues and tumor were very low. In Cit-L, CPT-11 and SN-38 were mainly detected in the liver and spleen. In IP6- and Cu-L, CPT-11 was strongly detected in the plasma, liver and spleen, and SN-38 in the plasma and liver. For the tumor concentration of CPT-11, IP6- and Cu-L showed 183- and 116-fold higher concentrations 24 h after administration than free CPT-11. For tumor concentrations of SN-38, IP6- and Cu-L showed 96- and 77-fold higher concentrations 24 h after administration than free CPT-11.

3.4. In vitro antitumor effect on Colon 26 tumor cells

IP-6 has been reported as an antineoplastic agent and increased the cytotoxic effect in breast tumor cells when combined with doxorubicin or tamoxifen [21]; therefore, we explored the co-treatment of CPT-11 plus IP-6 or SN-38 plus IP-6 to determine whether this treatment results in greater growth suppression or enhancement of cytotoxicity. The IC_{50} of IP-6 alone for Colon 26 cells was 0.27 mM (Fig. 4A), corresponding with the report that IP-6 inhibited cell growth at concentrations ranging from 10 μM to 1 mM in most mammalian tumor cells [26]. CPT-11 and CPT-11 plus 0.1 mM IP-6 did not exhibit cytotoxicity for Colon 26 cells (Fig. 4B). In contrast, SN-38 showed cytotoxicity for the cells ($IC_{50}=9.9$ nM), and SN-38 plus 0.1 mM IP-6 increased the cytotoxicity ($IC_{50}=8.5$ nM) (Fig. 4C). As a result, combination therapy of SN-38 plus IP-6 resulted in a significantly greater suppression of tumor growth than SN-38 alone, but combination therapy of CPT-11 plus IP-6 did not.

3.5. Antitumor effect on Colon 26 and COLO 320DM tumor xenografts

Antitumor activity of liposomal CPT-11 and free CPT-11 was evaluated following one or three intravenous injections into Colon 26 tumor-bearing mice. Protracted dosing schedules would be beneficial for S-phase active drugs like CPT-11. A dose of 60 mg/kg was considered the maximum tolerated dose of free CPT-11, because when free CPT-11 at a dose of 100 mg/kg was administered to mice bearing a Colon 26 tumor, the mice died after a few minutes, but not at 60 mg/kg (data not shown). Three injections of IP6-L at 20 mg/kg showed higher

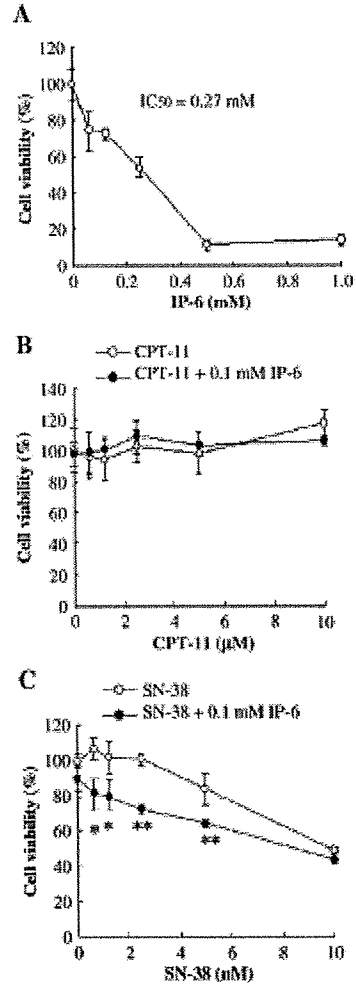

Fig. 4. Cytotoxicity of IP-6 (A) and the combination of CPT-11 (B) or SN-38 (C) for Colon 26 cells. Cells were treated with IP-6 at various concentrations and incubated for 72 h (A). In B and C, cells were treated with various concentrations of CPT-11 (B) and SN-38 (C) in the presence of 0.1 mM IP-6. Each result represents the mean ± S.D. ($n=3$). *$P<0.05$, **$P<0.01$, compared with cells treated with SN-38 alone.

antitumor activity than a single injection (Fig. 5A). Antitumor activity by liposomal CPT-11 seemed to depend on the injection frequency fixed at 60 mg/kg; therefore, triple injections of IP6-L were used thereafter.

Next, to examine the dose dependency of the antitumor effect, IP6-L was administered at doses of 10 and 20 mg/kg 3 times at three-day intervals. The tumor suppressive effect by IP6-L seemed to be dose-

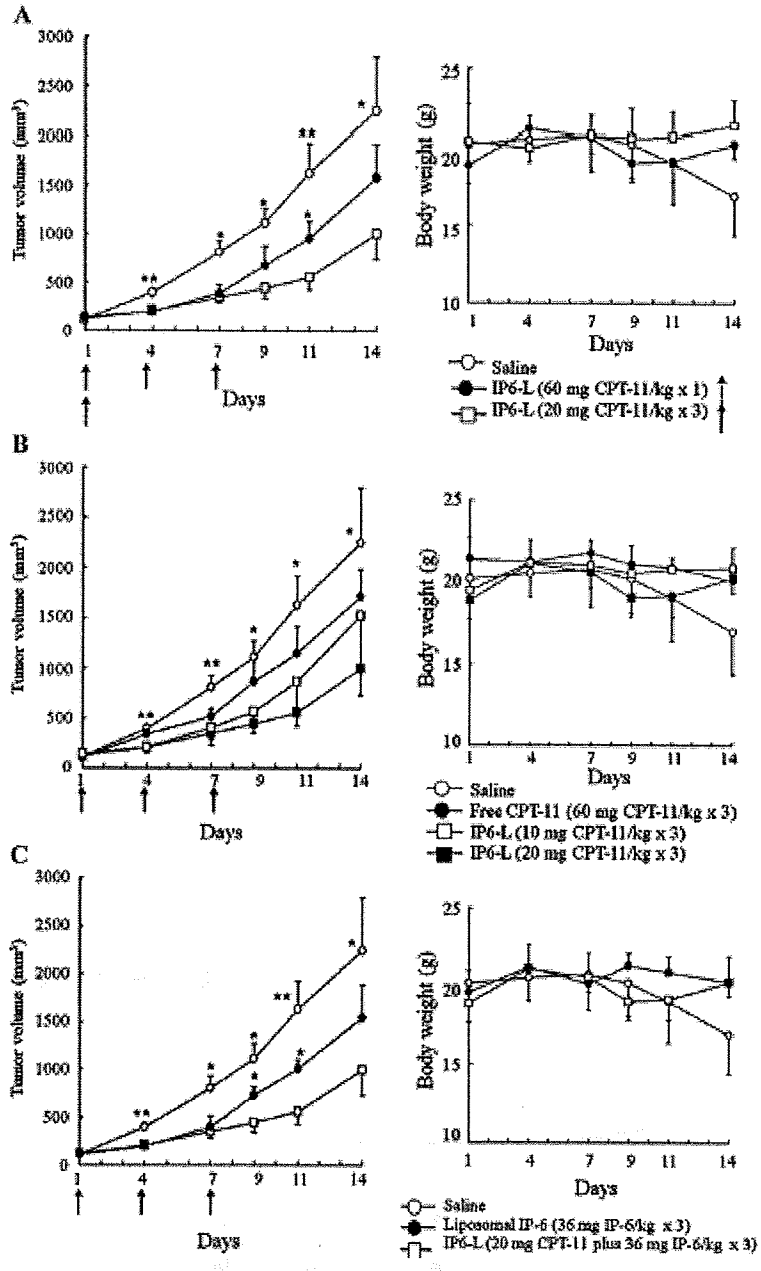

Fig. 5. Antitumor activity of IP6-L as determined in Colon 26 tumor. Antitumor activity and toxicity were assessed by measuring tumor volume and body weight change after intravenous injection of CPT-11. A, Saline (○) was intravenously administered on days 1, 4 and 7. IP6-L was administered by a single injection at 60 mg CPT-11/kg (●) on day 1 or triple injections of 20 mg CPT-11/kg (□) on days 1, 4 and 7. B, Saline (○), free CPT-11 (●) and IP6-L (□; 10 mg CPT-11/kg, ■; 20 mg CPT-11/kg) were administered on days 1, 4 and 7. C, Saline (○), liposomal IP-6 (●) and 20 mg/kg IP6-L (□) were administered on days 1, 4 and 7. Arrows indicate the day of drug injections. Each value represents the mean ± S.D. ($n = 4$). *$P < 0.05$, **$P < 0.01$, compared with mice injected with IP6-L (20 mg CPT-11/kg × 3).

dependent, and IP6-L administered at 20 mg/kg showed the highest tumor growth inhibition (Fig. 5B). Furthermore, IP6-L administered at 10 mg CPT-11/kg was superior in tumor suppression to free CPT-11 at 60 mg/kg. To examine the tumor suppressive effect of IP-6, liposomal IP-6 and IP6-L were injected into the tumors 3 times at 3-day intervals (Fig. 5C). Liposomal IP-6 (36 mg IP-6/kg) showed tumor growth inhibition, and IP6-L (20 mg CPT-11/kg plus 36 mg IP-6/kg) increased its tumor suppressive effect significantly on day 9 and 11. There were no remarkable differences in mice body weight changes after administration of IP6-L.

We investigated whether different loading methods of liposomal CPT-11 improved the therapeutic efficacy of CPT-11. The therapeutic benefits of free and liposomal CPT-11 were assessed in two advanced colon tumor models. We decided to use IP6- and Cu-L as liposomal CPT-11, because Cit-L did not circulate for long in blood and did not accumulate in the tumor (Figs. 2 and 3).

Mice bearing Colon 26 tumors were administered free CPT-11, and Cu- and IP6-L 3 times at a dose of 20 mg CPT-11/kg at 3-day intervals (Fig. 6A). Anticancer efficacy was significantly different for each CPT-11 formulation, and IP6-L-injected mice showed significant tumor growth inhibition compared to Cu-L and free CPT-11. The percentage of tumor growth inhibition (T/C%), which represents the mean difference (%) in tumor size for treated tumors (T) compared with control tumors (C), was calculated from relative tumor volume at day 15 in Colon 26 tumor. The calculated T/C treated with free CPT-11, Cu- and IP6-L in Colon 26 tumor was 75, 64 and 28 on day 15, respectively. We did not observe a significant loss of weight in mice administered Cu- and IP6-L on day 15 in spite of transiently loss of weight immediately after the repeated injections on day 10. This anticancer efficacy of IP6-L indicated that CPT-11 loaded into liposomes was released and co-encapsulated IP-6 increased CPT-11 activity.

Finally, COLO 320DM tumor xenografts were administered with free CPT-11, and Cu- and IP6-L 3 times at a dose of 20 mg/kg at 3-day intervals (Fig. 6B). The tumors in mice treated with IP6- and Cu-L gradually disappeared and were completely gone within 2 weeks after

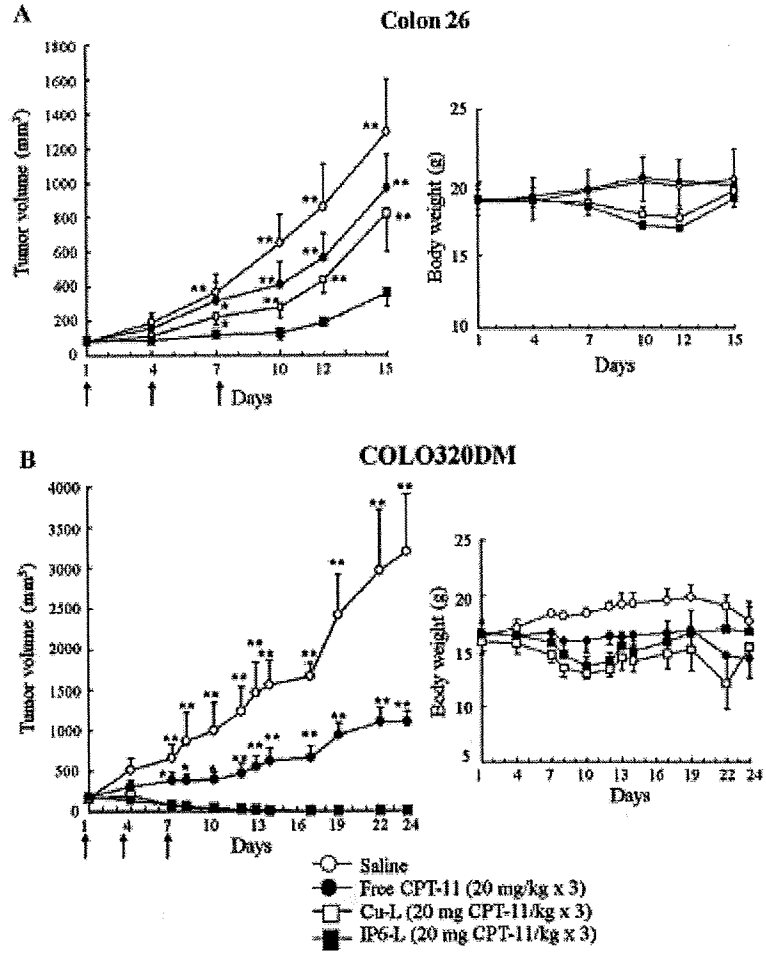

Fig. 6. Antitumor activity of liposomal CPT-11 as determined in Colon 26 tumor (A) and COLO 320DM tumor xenografts (B). Antitumor activity and toxicity were assessed by measuring tumor volume and body weight change after intravenous injection of free and liposomal CPT-11 (equivalent to 20 mg CPT-11/kg). Saline (○), free CPT-11 (●), Cu-L (□) and IP6-L (■) were administered on days 1, 4 and 7. Arrows indicate the day of drug injections. Each value represents the mean ± S.D. ($n = 4$). *$P < 0.05$, **$P < 0.01$, compared with mice injected with IP6-L.

the first administration. Body weight after administration of Cu- and IP6-L temporarily decreased but recovered after 2 weeks, indicating that the dose of liposomal CPT-11 may decrease in nude mice with a tumor to prevent side effects. It has been reported that COLO 320DM cells were sensitive to CPT-11, and even free CPT-11 could suppress tumor growth in COLO 320DM xenografts [27]. In this study, free CPT-11 exhibited significant tumor suppression compared with saline-injected mice, as previously reported [27]. The calculated T/C% values treated with free CPT-11, and Cu- and IP6-L in COLO 320DM xenografts were 40, 0.3 and 0.5 on day 14, respectively.

4. Discussion

In this study, we prepared IP6-L using a non-polymeric negatively charged compound, IP-6, for remote loading of CPT-11 into liposomes, and demonstrated that IP6-L had significantly superior anticancer activity to Cu-L in Colon 26 tumor and human COLO 320DM tumor xenografts. As loading methods for CPT-11 into liposomes, the pH gradient method by citrate and the ion-mediated encapsulation method with $CuSO_4$ were reported [9,10]. Therefore, we compared the loading efficiency of CPT-11 in liposomes loaded by IP-6 mediated methods (IP6-L) with those by citrate and $CuSO_4$-mediated methods (Cit-L, Cu-L). IP6- and Cu-L retained high loading efficiencies at a CPT-11 to total lipid ratio of 0.6. It is known that IP-6 is widely used as a chelator for cationic substrate [28] and copper can interact with CPT-11 [29]. The high loading efficiency of CPT-11 in IP6-L supposed that IP-6 may interact with CPT-11 in the liposome interior.

IP6-L prepared with 100–500 mM pH-unadjusted IP-6 solution (pH<2) was aggregated soon after preparation. When the pH of IP-6 solution was adjusted to 6.5 with TEA or NaOH, no aggregations were observed in the IP6-L (data not shown), but IP6-L with TEA showed higher loading efficiency than that with NaOH, indicating that TEA played an important role in remote loading of CPT-11 as it was previously reported that TEA gradient promoted CPT-11 encapsulation into liposomes [13]. As CPT-11 has a pKa of 8.1, it has a different population of both charged and uncharged molecules at pH 7.4 in extraliposomes and at pH 6.5 in intraliposomes; the ratios of charged to uncharged molecules of CPT-11 at pH 7.4 and 6.5 are 5.2 and 41, respectively. When CPT-11 is added to the outside of liposomal IP-6, the uncharged form translocates through the liposome bilayer to the intraliposome, and then changes to the charged form by proton shift from TEA [13]. The positively charged form of CPT-11 may interact with negatively charged phosphate residues of IP-6 and accumulate in liposomes; therefore, IP-6 adjusted with TEA was effective for remote loading of CPT-11.

The most striking observation in this study was the effectiveness of IP6-L in an animal model. The AUC of CPT-11 and SN-38 in IP6-L was significantly higher than that in Cu-L (Table 1), and IP6-L and Cu-L showed similarly high accumulations of CPT-11 and SN-38 in the tumor 24 h after administration (Fig. 3). The amount of SN-38 in the tumor after administration of Cu-L was similar to that in a previous report [30]. As antitumor effects, IP6-L exhibited a significantly higher tumor suppressive effect in Colon 26 tumors compared with Cu-L (Fig. 6A). Three injections of IP6-L at 20 mg CPT-11/kg showed higher antitumor activity than a single injection at 60 mg/kg, suggesting that multiple injections could improve the retention of CPT-11 and SN-38 in blood and induce high antitumor activity. In a COLO320DM tumor model, IP6-L also showed an effective antitumor effect as well as Cu-L (Fig. 6B), and the tumors completely disappeared.

Although the basis of the effect remains incompletely understood, two factors help to explain the result. First, IP6-L with CPT-11 stabilized by IP-6 showed prolonged circulation in the blood compared with free CPT-11 and Cu-L, resulting in high tumor exposure. The sustained release of CPT-11 from liposomes could prevent the saturation of carboxyesterase enzyme in the liver [30], enabling IP6-L to maintain high plasma SN-38 levels over the duration of the experiments. Here, since a relatively low dose (20 mg/kg) was used, the lack of a dose–response effect was observed. Second, IP-6 in IP6-L may exhibit synergic tumor suppression with SN-38 *in vivo* as combination treatment of SN-38 plus IP-6 significantly increased the cytotoxic effect on Colon 26 tumor cells. IP-6 has been found to cause G_1 cell cycle arrest [31], and to stimulate p53 and p21 expression, and to increase the expression of p21 in human colon tumor cell lines [19,20,32]. Exposure of IP-6 in tumor cells and xenografts resulted in a dose-dependent decrease in the expression of vascular endothelial growth factor (VEGF) [33,34]. Furthermore, long circulation in blood leads to increased accumulation of liposomal IP-6 in tumors by enhanced permeability and retention effects. Once IP-6 in IP6-L was accumulated in the tumor, IP-6 could function synergically with SN-38. We are currently investigating whether the activity of CPT-11 is increased *in vivo*, being mediated by a dual-action mechanism encompassing anti-vascular and direct tumor cell cytotoxicity actions of IP-6. Thus, CPT-11 in IP6-L was converted to SN-38 and then suppressed tumor growth in combination with IP-6 *in vivo*. According to our results, we supposed that IP6-L could increase antitumor activity by liposomal CPT-11 and IP-6.

5. Conclusions

We developed a novel loading method of CPT-11 into liposomes, which was mediated by IP-6 and triethanolamine. The loading efficiency of IP6-L was higher than those of Cit-L and similar to Cu-L. IP6-L showed significantly higher AUC than Cit-L and Cu-L, and showed significantly superior anticancer activity than Cu-L in Colon 26 tumors. Liposomal CPT-11 with IP-6 not only could achieve efficient loading at a high drug-to-lipid ratio but also enhanced its antitumor activity against colon tumors.

Acknowledgments

We thank Mr. Takumi Tanaka for his assistance with the experimental work. This study was supported in part by the Japan Health Sciences Foundation, by the Ministry of Education, Culture, Sports, Science and Technology of Japan, and by the Open Research Center Project.

References

[1] Y.H. Hsiang, H.Y. Wu, L.F. Liu, Topoisomerases: novel therapeutic targets in cancer chemotherapy, Biochem. Pharmacol. 37 (1988) 1801–1807.
[2] Y.H. Hsiang, L.F. Liu, Identification of mammalian DNA topoisomerase I as an intracellular target of the anticancer drug camptothecin, Cancer Res. 48 (1988) 1722–1726.
[3] Y.H. Hsiang, M.G. Lihou, L.F. Liu, Arrest of replication forks by drug-stabilized topoisomerase I-DNA cleavable complexes as a mechanism of cell killing by camptothecin, Cancer Res. 49 (1989) 5077–5082.
[4] L.B. Saltz, The role of irinotecan in colorectal cancer, Curr. Oncol. Rep. 1 (1999) 155–161.
[5] L.B. Saltz, J.V. Cox, C. Blanke, L.S. Rosen, L. Fehrenbacher, M.J. Moore, J.A. Maroun, S.P. Ackland, P.K. Locker, N. Pirotta, G.L. Elfring, L.L. Miller, Irinotecan plus fluorouracil and leucovorin for metastatic colorectal cancer. Irinotecan Study Group, N. Engl. J. Med. 343 (2000) 905–914.
[6] Y. Kawato, M. Aonuma, Y. Hirota, H. Kuga, K. Sato, Intracellular roles of SN-38, a metabolite of the camptothecin derivative CPT-11, in the antitumor effect of CPT-11, Cancer Res. 51 (1991) 4187–4191.
[7] Y. Kawato, T. Furuta, M. Aonuma, M. Yasuoka, T. Yokokura, K. Matsumoto, Antitumor activity of a camptothecin derivative, CPT-11, against human tumor xenografts in nude mice, Cancer Chemother. Pharmacol. 28 (1991) 192–198.
[8] F. Lavelle, M.C. Bissery, S. Andre, F. Roquet, J.F. Riou, Preclinical evaluation of CPT-11 and its active metabolite SN-38, Semin. Oncol. 23 (1996) 11–20.
[9] T.H. Chou, S.C. Chen, I.M. Chu, Effect of composition on the stability of liposomal irinotecan prepared by a pH gradient method, J. Biosci. Bioeng. 95 (2003) 405–408.
[10] E. Ramsay, J. Alnajim, M. Anantha, A. Taggar, A. Thomas, K. Edwards, G. Karlsson, M. Welch, M. Bally, Transition metal-mediated liposomal encapsulation of irinotecan (CPT-11) stabilizes the drug in the therapeutically active lactone conformation, Pharm. Res. 23 (2006) 2799–2808.
[11] C.L. Messerer, E.C. Ramsay, D. Waterhouse, K. Ng, E.M. Simms, N. Hamayun, P. Tardi, L.D. Mayer, M.B. Bally, Liposomal irinotecan: formulation development and therapeutic assessment in murine xenograft models of colorectal cancer, Clin. Cancer Res. 10 (2004) 6638–6649.

[12] E. Ramsay, J. Alnajim, M. Anantha, J. Zastre, H. Yan, M. Webb, D. Waterhouse, M. Bally, A novel liposomal irinotecan formulation with significant anti-tumour activity: use of the divalent cation ionophore A23187 and copper-containing liposomes to improve drug retention, Eur. J. Pharm. Biopharm. (2007).
[13] A. Dicko, P. Tardif, X. Xie, L. Mayer, Role of copper gluconate/triethanolamine in irinotecan encapsulation inside the liposomes, Int. J. Pharm. 337 (2007) 219–228.
[14] FM. Walsh, F.J. Crosson, M. Bayley, J. McReynolds, B.J. Pearson, Acute copper intoxication. Pathophysiology and therapy with a case report, Am. J. Dis. Child. 131 (1977) 149–151.
[15] D.G. Barceloux, Copper, J. Toxicol. Clin. Toxicol. 37 (1999) 217–230.
[16] S. Kawanishi, S. Inoue, K. Yamamoto, Hydroxyl radical and singlet oxygen production and DNA damage induced by carcinogenic metal compounds and hydrogen peroxide, Biol. Trace Elem. Res. 21 (1989) 367–372.
[17] D.C. Drummond, C.O. Noble, Z. Guo, K. Hong, J.W. Park, D.B. Kirpotin, Development of a highly active nanoliposomal irinotecan using a novel intraliposomal stabilization strategy, Cancer Res. 66 (2006) 3271–3277.
[18] J.S. Diallo, B. Pelant, L. Lessard, N. Delvoye, P.C. Le, A.M. Mes-Masson, F. Saad, An androgen-independent androgen receptor function protects from inositol hexakisphosphate toxicity in the PC3/PC3(AR) prostate cancer cell lines, Prostate 66 (2006) 1245–1256.
[19] L. Wegiarz, L. Molin, A. Orchel, B. Parfiniewicz, Z. Dzierzewicz, Quantitative analysis of the level of p53 and p21(WAF1) mRNA in human colon cancer HT-29 cells treated with inositol hexaphosphate, Acta Biochim. Pol. 53 (2006) 349–356.
[20] I.T. Saied, A.M. Shamsuddin, Up-regulation of the tumor suppressor gene p53 and WAF1 gene expression by IP6 in HT-29 human colon carcinoma cell line, Anticancer Res. 18 (1998) 3479–3484.
[21] K. Tantivejkul, I. Vucenik, J. Eliseman, A.M. Shamsuddin, Inositol hexaphosphate (IP6) enhances the anti-proliferative effects of adriamycin and tamoxifen in breast cancer, Breast Cancer Res. Treat. 79 (2003) 301–312.
[22] H.G. Yu, Y.W. Ai, L.L. Yu, X.D. Zhou, J. Liu, J.H. Li, X.M. Xu, S. Liu, J. Chen, F. Liu, Y.L. Qi, Q. Deng, J. Cao, S.Q. Liu, H.S. Luo, J.P. Yu, Phosphoinositide 3-kinase/Akt pathway plays an important role in chemoresistance of gastric cancer cells against etoposide and doxorubicin induced cell death, Int. J. Cancer 122 (2008) 433–443.
[23] Y. Maitani, S. Igarashi, M. Sato, Y. Hattori, Cationic liposome (DC-Chol/DOPE= 1:2) and a modified ethanol injection method to prepare liposomes, increased gene expression, Int. J. Pharm. 342 (2007) 33–39.
[24] Y. Tajima, Biological reference data book on experimental animals, soft science, Tokyo (1989) 96.
[25] S. Takenoto, K. Yamaoka, M. Nishikawa, Y. Takakura, Histogram analysis of pharmacokinetic parameters by bootstrap resampling from one-point sampling data in animal experiments, Drug Metab. Pharmacokinet. 21 (2006) 458–464.
[26] A.M. Shamsuddin, Metabolism and cellular functions of IP6: a review, Anticancer Res. 19 (1999) 3733–3736.
[27] W.J. Jansen, R. Zwart, S.T. Hulscher, G. Giaccone, H.M. Pinedo, E. Boven, CPT-11 in human colon-cancer cell lines and xenografts: characterization of cellular sensitivity determinants, Int. J. Cancer 70 (1997) 335–340.
[28] U.P. Rodrigues-Filho, S. Vaz Jr., M.P. Felicissimo, M. Scarpellini, D.R. Cardoso, R.C. Vinhas, R. Landers, J.F. Schneider, R.R. McGarvey, M.L. Andersen, I.H. Skibsted, Heterometallic manganese/zinc-phytate complex as a model compound for metal storage in wheat grains, J. Inorg. Biochem. 99 (2005) 1973–1982.
[29] A.S. Taggar, J. Alnajim, M. Anantha, A. Thomas, M. Webb, E. Ramsay, M.B. Bally, Copper-topotecan complexation mediates drug accumulation into liposomes, J. Control. Release 114 (2006) 78–88.
[30] E.C. Ramsay, M. Anantha, J. Zastre, M. Meija, J. Zenderhuiz, D. Strutt, M.S. Webb, D. Waterhouse, M.B. Bally, Irinophore C: a liposome formulation of irinotecan with substantially improved therapeutic efficacy against a panel of human xenograft tumors, Clin. Cancer Res. 14 (2008) 1208–1217.
[31] Y.M. El-Sherbiny, M.C. Cox, Z.A. Ismail, A.M. Shamsuddin, I. Vucenik, G0/G1 arrest and S phase inhibition of human cancer cell lines by inositol hexaphosphate (IP6), Anticancer Res. 21 (2001) 2393–2403.
[32] I. Vucenik, A.M. Shamsuddin, Cancer inhibition by inositol hexaphosphate (IP6) and inositol: from laboratory to clinic, J. Nutr. 133 (2003) 3778S–3784S.
[33] R.P. Singh, G. Sharma, G.H. Mallikarjuna, S. Dhanalakshmi, C. Agarwal, R. Agarwal, In vivo suppression of hormone-refractory prostate cancer growth by inositol hexaphosphate: induction of insulin-like growth factor binding protein-3 and inhibition of vascular endothelial growth factor, Clin. Cancer Res. 10 (2004) 244–250.
[34] I. Vucenik, A. Passaniti, M.L. Vitolo, K. Tantivejkul, P. Eggleton, A.M. Shamsuddin, Anti-angiogenic activity of inositol hexaphosphate (IP6), Carcinogenesis 25 (2004) 2115–2123.

articles

molecular pharmaceutics

Higher Liposomal Membrane Fluidity Enhances the in Vitro Antitumor Activity of Folate-Targeted Liposomal Mitoxantrone

Kumi Kawano, Eri Onose, Yoshiyuki Hattori, and Yoshie Maitani*

Institute of Medicinal Chemistry, Hoshi University, Ebara 2-4-41, Shinagawa-ku, Tokyo 142-8501, Japan

Received June 23, 2008; Revised Manuscript Received November 5, 2008; Accepted November 17, 2008

Abstract: The efficacy of folate-targeted liposomal drug delivery has not been fully achieved in part because of the slow release of the encapsulated drugs following uptake of the liposomes by target cells. Since liposomal mitoxantrone (MXN) composed of lipids with high fluidity was reported to achieve strong anticancer effects in vivo, we hypothesized that folate-targeted liposomal MXN uptake via folate receptor (FR)-mediated endocytosis could effectively release drugs into the endosomal compartment. Folate-targeted liposomal MXN was prepared using two lipids with different fluidities. MXN was released slowly from all types of liposome into PBS, indicating that the cellular uptake of MXN was considered to be in the liposomal form. Folate-targeted liposomes with high fluidity exhibited lower cellular uptake of loaded FITC-labeled dextran into FR (+) KB cells, but, when MXN was loaded, higher cytotoxicity than liposomes with lower fluidity. On the other hand, the cellular uptake of non-folate liposomes was not affected by the membrane fluidity, but higher cytotoxicity was observed in liposomal MXN with high fluidity, which suggested a higher rate of release of the drug from the liposomes. High levels of cytotoxic activity were achieved with folate-targeted liposomal MXN though the cellular uptake rate was restricted by selecting liposomes with higher lipid membrane fluidity. This finding provides a new insight into folate-targeted carrier drug delivery.

Keywords: Liposome; folate targeting; mitoxantrone; membrane fluidity

1. Introduction

Liposome formulations have been developed to enhance the therapeutic activity of anticancer agents. To increase the therapeutic effect on tumors, various targeting ligands have been investigated as tumor targeted drug carriers. Folate receptor (FR), a 38 kDa glycosyl−phosphatidylinositol−anchored glycoprotein, is overexpressed in many human cancer cells, including malignancies of the ovary, mammary gland, lung, kidney, and throat, but are expressed minimally in normal tissues.[1,2] Therefore, FR can serve as a functional tumor-specific receptor. Folic acid, a high-affinity ligand for FR, and its conjugate retain its receptor binding and endocytosis properties with FR positive cancer cells; FR-targeted liposome carriers have shown both selective binding and uptake. Liposomes conjugated to the folate ligand via a polyethylene glycol (PEG) spacer have been used to deliver chemotherapeutic agents.[3,4] It has already been shown that the length of the PEG linker chain and the amount of folate ligand are important for liposomes to be internalized fol-

* Corresponding author. Mailing address: Institute of Medicinal Chemistry, Hoshi University, Ebara 2-4-41, Shinagawa, Tokyo, 142-8501 Japan. Tel and fax: +81-3-5498-5048. E-mail: yoshie@hoshi.ac.jp.

(1) Toffoli, G.; Cernigoi, C.; Russo, A.; Gallo, A.; Bagnoli, M.; Boiocchi, M. Overexpression of folate binding protein in ovarian cancers. *Int. J. Cancer* **1997**, *74* (2), 193–198.

(2) Weitman, S. D.; Lark, R. H.; Coney, L. R.; Fort, D. W.; Frasca, V.; Zurawski, V. R., Jr.; Kamen, B. A. Distribution of the folate receptor GP38 in normal and malignant cell lines and tissues. *Cancer Res.* **1992**, *52* (12), 3396–3401.

(3) Gabizon, A.; Horowitz, A. T.; Goren, D.; Tzemach, D.; Shmeeda, H.; Zalipsky, S. In vivo fate of folate-targeted polyethylene-glycol liposomes in tumor-bearing mice. *Clin. Cancer Res.* **2003**, *9* (17), 6551–6559.

10.1021/mp800069c CCC: $40.75 © 2009 American Chemical Society
Published on Web 12/15/2008

lowing recognition by FR[5] and uptake into cancer cells.[6] Longer PEG spacers (MW 5000) and lower concentrations of folate ligand were more effective for FR-targeting in vitro.[7]

Unfortunately, the efficacy of folate-targeted liposomal drug delivery has not achieved its full potential, in part because of the slow release of the encapsulated drugs following uptake of the liposomes by target cells. In order to overcome this obstacle, pH-sensitive liposomes have been developed.[8] However, there are few reports to our knowledge on the effect of lipid composition of folate-targeted liposomes on FR-targeting in regard to liposomal membrane fluidity. Focusing on lipid composition in drug release, it has been reported that liposomal mitoxantrone (MXN) composed of lipids with higher fluidity showed higher efficacy in vivo,[9] and MXN release from liposomes became the dominant factor contributing to therapeutic activity in vivo.[10,11] The lipid composition of liposomes might affect the cellular association and release of MXN into the cytoplasm differently. The possible explanations for this have not yet been clarified in vitro. Furthermore, from the in vivo results with MXN,[12] it was predicted that the mixing of lipids with shorter alkyl tails (<C18) in liposomes during the cellular uptake process within the endosome will promote endosomal membrane fluidity and enhance drug release. Therefore, in this study it was hypothesized that folate-targeted liposomal MXN composed of lipids with high fluidity could achieve stronger anticancer effects by higher uptake by FR-mediated endocytosis and then rapid release of the drug from the endosomal compartment.

Although anthracyclines, such as MXN and doxorubicin (DXR), have a similar structure, they have significantly different octanol/buffer partition coefficient.[13] Liposomal DXR has been extensively investigated in this area, and consequently it was selected as a control. This study investigated the drug release, cellular association, and in vitro antitumor activity of folate-targeted liposomal MXN composed of two lipids with different fluidities compared with liposomal DXR in FR-positive KB cells, which is a human nasopharyngeal cell line.

2. Materials and Methods

2.1. Materials. Hydrogenated soybean phosphatidylcholine (HSPC) and dimyristoyl phosphatidylcholine (DMPC) were obtained, and amino-poly(ethyleneglycol)-distearylphosphatidylethanolamine (amino-PEG-DSPE, PEG mean molecular weight 5,000) was a kind gift from NOF Corp. (Tokyo, Japan). Egg phosphatidylcholine (EPC) was purchased from Q. P. Co., Ltd. (Tokyo, Japan). MXN hydrochloride was a kind gift from Wyeth K.K. (Tokyo, Japan). DXR hydrochloride and cholesterol (Ch) were purchased from Wako Pure Chemical Industries Ltd. (Osaka, Japan). 1,6-Diphenyl-1,3,5-hexatriene (DPH) was purchased from Aldrich Chemical Co. (Milwaukee, WI). Dextran-fluorescein isothiocyanate (D-FITC, molecular weight ~4,000) was purchased from Sigma Chemical Co. (St Louis, MO). Folate-PEG_{5000}-DSPE conjugate of folic acid was synthesized from amino-PEG-DSPE as reported previously.[5,14] Folate-deficient RPMI-1640 medium and fetal bovine serum (FBS) were obtained from Invitrogen Corp. (Carlsbad, CA). Other reagents used in this study were of reagent grade.

2.2. Preparation of Folate-Targeted Liposome. 2.2.1. Folate-Targeted Liposome Preparation. Liposomes were prepared from HSPC/Ch = 55/45 (mol/mol), DMPC/Ch = 55/45 (mol/mol), and EPC/Ch = 55/45 (mol/mol); HSPC-L, DMPC-L, and EPC-L, respectively, by a dry-film method as reported previously.[15] Briefly, all lipids were dissolved in chloroform, which was then removed by evaporation to leave a thin lipid film. The thin film was hydrated with citrate buffer (300 mM, adjusted to pH 4.0 with NaOH) and

(4) Pan, X. Q.; Wang, H.; Lee, R. J. Antitumor activity of folate receptor-targeted liposomal doxorubicin in a KB oral carcinoma murine xenograft model. *Pharm. Res.* **2003**, *20* (3), 417–422.

(5) Gabizon, A.; Horowitz, A. T.; Goren, D.; Tzemach, D.; Mandelbaum-Shavit, F.; Qazen, M. M.; Zalipsky, S. Targeting folate receptor with folate linked to extremities of poly(ethylene glycol)-grafted liposomes: in vitro studies. *Bioconjugate Chem.* **1999**, *10* (2), 289–298.

(6) Saul, J. M.; Annapragada, A.; Natarajan, J. V.; Bellamkonda, R. V. Controlled targeting of liposomal doxorubicin via the folate receptor in vitro. *J. Controlled Release* **2003**, *92* (1−2), 49–67.

(7) Kawano, K.; Maitani, Y. Effect of PEG spacer length and ligand density on folate receptor targeting of liposomal doxorubicin. *Drug Dev. Ind. Pharm.*, submitted.

(8) Turk, M. J.; Reddy, J. A.; Chmielewski, J. A.; Low, P. S. Characterization of a novel pH-sensitive peptide that enhances drug release from folate-targeted liposomes at endosomal pHs. *Biochim. Biophys. Acta* **2002**, *1559* (1), 56–68.

(9) Lim, H. J.; Masin, D.; McIntosh, N. L.; Madden, T. D.; Bally, M. B. Role of drug release and liposome-mediated drug delivery in governing the therapeutic activity of liposomal mitoxantrone used to treat human A431 and LS180 solid tumors. *J. Pharmacol. Exp. Ther.* **2000**, *292* (1), 337–345.

(10) Lim, H. J.; Masin, D.; Madden, T. D.; Bally, M. B. Influence of drug release characteristics on the therapeutic activity of liposomal mitoxantrone. *J. Pharmacol. Exp. Ther.* **1997**, *281* (1), 566–573.

(11) Wu, M.; Gunning, W.; Ratnam, M. Expression of folate receptor type alpha in relation to cell type, malignancy, and differentiation in ovary, uterus, and cervix. *Cancer Epidemiol. Biomarkers Prev.* **1999**, *8* (9), 775–782.

(12) Adlakha-Hutcheon, G.; Bally, M. B.; Shew, C. R.; Madden, T. D. Controlled destabilization of a liposomal drug delivery system enhances mitoxantrone antitumor activity. *Nat. Biotechnol.* **1999**, *17* (8), 775–779.

(13) Regev, R.; Yeheskely-Hayon, D.; Katzir, H.; Eytan, G. D. Transport of anthracyclines and mitoxantrone across membranes by a flip-flop mechanism. *Biochem. Pharmacol.* **2005**, *70* (1), 161–169.

(14) Shiokawa, T.; Hattori, Y.; Kawano, K.; Ohguchi, Y.; Kawakami, H.; Toma, K.; Maitani, Y. Effect of polyethylene glycol linker chain length of folate-linked microemulsions loading aclacinomycin A on targeting ability and antitumor effect in vitro and in vivo. *Clin. Cancer Res.* **2005**, *11* (5), 2018–2025.

(15) Horowitz, A. T.; Barenholz, Y.; Gabizon, A. A. In vitro cytotoxicity of liposome-encapsulated doxorubicin: dependence on liposome composition and drug release. *Biochim. Biophys. Acta* **1992**, *1109* (2), 203–209.

sonicated to decrease the size. The folate ligand was inserted into preformed liposomes; HSPC-L and DMPC-L, by incubation with an aqueous dispersion of folate-PEG$_{5000}$-DSPE (0.03 mol% of total lipid) at 60 °C for 1 h (F/HSPC-L and F/DMPC-L, respectively). The resulting mean diameter of the liposomes was about 130 nm with a narrow size distribution (polydispersity <0.3), as determined by a dynamic light scattering method (ELS-Z2, Otsuka Electronics Co., Ltd., Osaka, Japan) at 25 °C after diluting the liposome suspension with water.

2.2.2. Preparation of Folate-Targeted Liposomal MXN and DXR. Folate-targeted liposomes were actively loaded with MXN[9,10] and DXR[16] by a pH gradient method. After the external pH was adjusted to pH 7.4, folate-targeted liposomes were incubated with MXN (drug:lipid = 1:10, wt/wt) at 60 °C for 20 min, or incubated with DXR (drug:lipid = 1:5, wt/wt) at 60 °C for 25 min. The loading efficiencies of MXN and DXR were determined by separating the unencapsulated drug from the encapsulated drug on a Sephadex G-50 column with saline as a mobile phase. MXN and DXR concentrations were determined by measuring absorbance at 608 and 480 nm, respectively (UV-1700 Pharmaspec, Shimadzu Co., Kyoto, Japan).

2.2.3. Preparation of Folate-Targeted Liposome Encapsulating D-FITC. D-FITC encapsulating liposomes were prepared by hydration of lipids with 15 mM HEPES buffer (pH 7.0) containing 30 mg/mL (3%) D-FITC and sonication. The folate ligand was inserted into preformed liposomes as described in section 2.2.1, Folate-Targeted Liposome Preparation. The liposomes were then dialyzed against HEPES buffer without D-FITC at room temperature until the dialysis buffer was fluorescein free.[17]

2.3. In Vitro Drug Release. The release of MXN and DXR from liposomes in a dialysis tube was measured using seamless cellulose tube membranes (Viskase Sales Corp., IL) with a molecular weight cutoff of 12,000–14,000. The initial concentrations of MXN and DXR were 450 μg/mL and 500 μg/mL, respectively. The sample volume in the dialysis tube was 1 mL of liposomal MXN or DXR with 1 mL of FBS to examine the influence of protein, and the sink volumes were 100 and 200 mL of phosphate-buffered saline at pH 7.4 (PBS) for MXN and DXR, respectively, at 37 °C.[18] The MXN concentration was analyzed using an HPLC column for analysis.[19] Methylene blue was used as the internal standard (i.s.). The HPLC system was composed of an LC-20AT pump (Shimadzu Co.), SIL-20A autoinjector (Shimadzu Co.), SPD-M20A UV–visible detector (Shimadzu Co.), and a YMC-PACK ODS-AA-302, 150 × 4.6 mm i.d. column (YMC Co., Ltd., Kyoto, Japan). The isocratic mobile phase was 29:71 (v/v) acetonitrile:ammonium formate (160 mM) with hexanesulfonic acid (35 mM), adjusted to pH 2.7 with formic acid, running at a flow rate of 1.0 mL/min. The i.s. and MXN were detected by absorbance at 655 nm. The DXR concentration was analyzed using a fluorophotometer (Wallac 1420 ARVOsx multilabel counter, Perkin-Elmer Life Science, Tokyo, Japan) with excitation and emission wavelengths of 485 and 535 nm, respectively.

2.4. Fluorescence Anisotropy Measurements. The precise method of fluorescence anisotropy measurement was as reported previously.[20] The phospholipid bilayer was labeled with DPH by adding 10 μL of 10 mM freshly prepared DPH stock solution in tetrahydrofuran to 1000 μL of liposome suspension and then incubated at 37 °C for 2 h in the dark to complete the labeling. The fluorescence anisotropy of DPH in liposomes was measured with a fluorescence spectrophotometer (Hitachi F-450, Hitachi Co. Ltd., Tokyo, Japan) at 15–45 °C. The excitation and emission wavelengths used for DPH were 351 and 430 nm, respectively. The effect of temperature on the fluorescence anisotropy of DPH was measured at a heating rate of 1 °C /min. The steady-state fluorescent anisotropy was calculated using the following equation: $r = (I_{VV} - I_{VH})/(I_{VV} + 2I_{VH})$ where r is anisotropy and I_{VV} and I_{VH} are the intensity measured in directions parallel and perpendicular to the polarized excitation light, respectively.

2.5. Cell Culture. KB cells were obtained from the Cell Resource Center for Biomedical Research, Tohoku University (Miyagi, Japan). The human lung adenocarcinoma A549 cell line was kindly provided by OncoTherapy Science, Inc. (Kanagawa, Japan). The cells were cultured in folate-deficient RPMI-1640 medium containing 10% heat-inactivated FBS and 50 μg/mL kanamycin sulfate in a humidified atmosphere containing 5% CO_2 at 37 °C.

2.6. Determination of Cellar Uptake of D-FITC-Encapsulating Liposomes. KB cells were prepared by plating 3×10^5 cells/well in a 6-well culture plate 1 day before the assay. Cells were incubated with D-FITC-encapsulating liposomes containing 100 μg/mL lipids in 2 mL of folate-deficient RPMI-1640 medium containing 10% heat-inactivated FBS for 2 h at 37 °C. After incubation, the cells were washed two times with PBS at pH 7.4, and lysed with PBS containing 0.2% Triton X-100. Associated amounts of D-FITC were measured using a fluorophotometer (Wallac 1420 ARVOsx multilabel counter)

(16) Lee, R. J.; Low, P. S. Folate-mediated tumor cell targeting of liposome-entrapped doxorubicin in vitro. *Biochim. Biophys. Acta* **1995**, *1233* (2), 134–144.

(17) Shmeeda, H.; Mak, L.; Tzemach, D.; Astrahan, P.; Tarshish, M.; Gabizon, A. Intracellular uptake and intracavitary targeting of folate-conjugated liposomes in a mouse lymphoma model with up-regulated folate receptors. *Mol. Cancer Ther.* **2006**, *5* (4), 818–824.

(18) Johnston, M. J.; Semple, S. C.; Klimuk, S. K.; Edwards, K.; Eisenhardt, M. L.; Leng, E. C.; Karlsson, G.; Yanko, D.; Cullis, P. R. Therapeutically optimized rates of drug release can be achieved by varying the drug-to-lipid ratio in liposomal vincristine formulations. *Biochim. Biophys. Acta* **2006**, *1758* (1), 55–64.

(19) Johnson, J. L.; Ahmad, A.; Khan, S.; Wang, Y. F.; Abu-Qare, A. W.; Ayoub, J. E.; Zhang, A.; Ahmad, I. Improved liquid chromatographic method for mitoxantrone quantification in mouse plasma and tissues to study the pharmacokinetics of a liposome entrapped mitoxantrone formulation. *J. Chromatogr. B* **2004**, *799*, 149–155.

(20) Maitani, Y.; Katayama, S.; Kawano, K.; Hayama, A.; Toma, K. Artificial Lipids Stabilized Camptothecin Incorporated into Liposomes. *Biol. Pharm. Bull.* **2008**, *31* (5), 990–993.

with excitation and emission wavelengths of 485 and 535 nm, respectively.[21] The cellular uptake of D-FITC was quantified by the fluorescence of the cell lysate. The amount of cellular uptake was calculated using the following equation:

$$\text{dose}(\%) = \frac{\text{cellular uptake of D-FITC (mg)}}{\text{applied D-FITC (mg)}} \times 100 \quad (1)$$

2.7. Flow Cytometry Analysis. KB and A549 cells were prepared by plating 3×10^5 cells/well or 1.5×10^5 cells/well, respectively, in a 6-well culture plate 1 day before assaying. Cells were incubated with D-FITC-encapsulating liposomes containing 100 μg/mL lipids diluted in 2 mL of folate-deficient RPMI-1640 medium containing 10% heat-inactivated FBS for 2 h at 37 °C, with non-folate or folate-targeted liposomes. After incubation, the cells were washed with cold PBS two times, detached with 0.05% trypsin, and then suspended in PBS containing 0.1% bovine serum albumin and 1 mM EDTA. The suspended cells were directly introduced into a FACSCalibur flow cytometer (Becton Dickinson, San Jose, CA) equipped with a 488 nm argon ion laser. Data for 10,000 fluorescent events were obtained by recording forward scatter and side scatter with 530/30 nm fluorescence. The autofluorescence of cells was taken as a control.

2.8. Cytotoxicity Study. KB cells were prepared by plating 1×10^4 cells in a 96-well culture plate 1 day before the experiment. Cells were then incubated with liposomes containing 0.02−200 μg/mL MXN or 0.01−100 μg/mL DXR diluted in folate-deficient RPMI-1640 medium containing 10% heat-inactivated FBS for 2 h at 37 °C. After incubation, the cells were washed with PBS and cultured in fresh medium containing 10% heat-inactivated FBS until 48 h. Cytotoxicity was determined using the WST-8 assay (Dojindo Laboratories, Kumamoto, Japan), based on enzymatic reduction of a tetrazolium salt, WST-8, to water-soluble formazan. The number of viable cells was then determined by absorbance measured at 450 nm using an automated plate reader (BioRad, CA).

2.9. Confocal Microscopy. After incubation with D-FITC-encapsulating liposome for 24 h or liposomal DXR containing 100 μg/mL lipids for 1, 2, 6 and 24 h as described in section 2.6, the medium was removed, and the cells were washed three times with PBS and fixed with 10% formaldehyde in PBS at 37 °C for 20 min. Then, the cells were coated with Aqua Poly/Mount (Polyscience, Warrington, PA) to prevent fading and covered with coverslips. The fixed cells were observed with a Radiance 2100 confocal laser scanning microscope (BioRad) with an excitation wavelength of 488 nm and an emission wavelength at 530 nm with a filter HQ515/30.

2.10. Statistical Analysis. Statistical comparisons were performed using Student's *t*-test. *P* values less than 0.05 were considered significant.

(21) Kawano, K.; Nakamura, K.; Hayashi, K.; Nagai, T.; Takayama, K.; Maitani, Y. Liver targeting liposomes containing beta-sitosterol glucoside with regard to penetration-enhancing effect on HepG2 cells. *Biol. Pharm. Bull.* **2002**, *25* (6), 766–770.

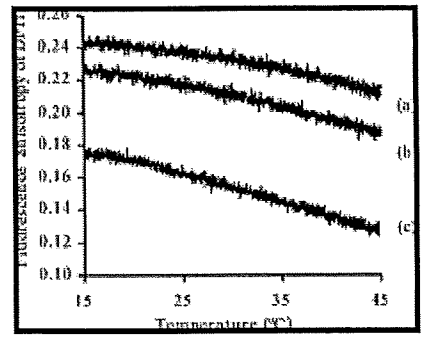

Figure 1. Temperature dependency of fluorescence anisotropy of DPH in liposomes. (a) HSPC-L, (b) DMPC-L, and (c) EPC-L.

3. Results and Discussion

3.1. Characterization of Liposomes. In this study, four types of liposome composed of either HSPC/Ch or DMPC/Ch were prepared with non-folate and folate-targeted liposomes. Folate-targeted liposomes were coated with 0.03 mol % folate-PEG_{5000}-DSPE because this modification showed the highest cellular uptake in KB cells (data not shown) as reported previously.[7] Both HSPC-L and DMPC-L were efficiently modified with folate-PEG_{5000}-DSPE of which insertion efficiency was 91.4% and 95.9%, respectively.

The use of the pH gradient method gave a high loading efficiency of MXN and DXR > 95% at a drug-to-total lipid ratio of 1:10 (wt:wt) and of 1:5 (wt:wt), respectively. The average particle diameter of each liposome in water was approximately 130 nm. The loading efficiency of liposomal MXN and DXR did not change significantly for at least 1 month at 4 °C in the dark.

The phase-transition temperature (T_m) of the phospholipid component influences drug retention. In general, liposomal membranes are more permeable through high membrane fluidity when the incubation temperature is above the T_m. To investigate the membrane fluidity of liposomes, fluorescence anisotropy studies were performed using the fluorescent probe DPH, which distributes deeply into the hydrophobic interior of liposomes. Anisotropy increased in the order EPC-L < DMPC-L < HSPC-L (Figure 1), which reflected the decreasing trend in membrane fluidity. This finding that liposomes composed of Ch and lipids with low T_m value exhibited higher liposomal membrane fluidity corresponded well with the inherent T_m values of EPC, DMPC, and HSPC of −10 °C, 23 °C, and 50−60 °C, respectively.

3.2. Stability of Liposomal MXN or DXR. Stability of liposomal MXN or DXR formulations was evaluated from drug release. The release assay of liposome suspension with 50% FBS is based on dialysis against a large volume of PBS to mimic the condition of liposomes incubated with cells. Under these conditions, whereas <45% free-MXN release was observed over a 48 h incubation period at 37 °C, <2.5% MXN release was observed from all liposomal formulations

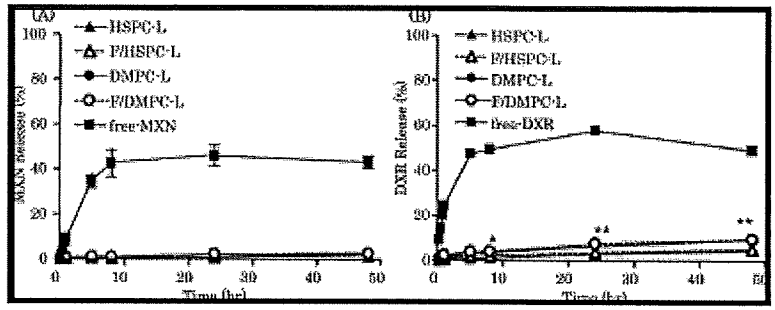

Figure 2. MXN (A) or DXR (B) release from liposomal MXN or DXR with FBS at 37 °C into PBS (pH 7.4). Each value represents mean ± SD (n = 3). *P < 0.05, **P < 0.01 for F/HSPC-L compared with F/DMPC-L and for HSPC-L compared with DMPC-L.

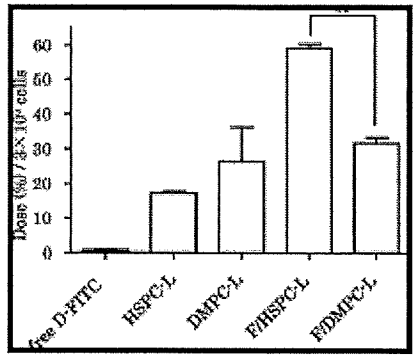

Figure 3. Cellular uptake of liposomes encapsulating D-FITC with KB cells 2 h at 37 °C after incubation by measuring the amount of D-FITC in the cells. Each value represents mean ± SE (n = 3). **P < 0.01 for F/HSPC-L compared with F/DMPC-L.

(Figure 2A). This result was consistent with MXN release studies in vitro that demonstrated no difference in drug release from liposomal formulations composed of distearyl phosphatidylcholine (DSPC) and DMPC[10] or that of dioleyl phosphatidylcholine and cardiolipin.[22] Different T_m values of the phospholipid species did not markedly affect MXN release. On the other hand, different DXR release rates were observed from different liposomal formulations. The release of DXR from both DMPC-L and F/DMPC-L exhibited a significantly more rapid release behavior than HSPC-L and F/HSPC-L, respectively, over 8 h (P < 0.05) (Figure 2B). This finding corresponded with the previous report that liposomes with higher T_m appeared to be more stable in PBS at 37 °C indicating T_m is directly proportional to stability.[23]

Concerning the difference in drug release from liposomes, MXN was released more slowly than DXR (Figure 2A,B). This finding adds to the report that liposomal MXN activity requires a modified lipid composition to promote release of the drug and improve efficiency.[10] The liposomal stability of MXN appears to be higher than that of DXR, using the current liposome formulations, supported by the report that more lipophilic MXN exhibited higher affinity toward liposome membranes compared to DXR.[13]

3.3. Cellular Uptake of Folate-Targeted Liposomes Encapsulating D-FITC. The cellular uptake of folate-targeted liposomes encapsulating D-FITC was investigated by incubation with FR (+) KB or FR (−) A549 cells both by measuring D-FITC in cells and by flow cytometry. Here D-FITC was used instead of MXN because MXN is not fluorescent and therefore its detection level was low. Moreover, since it is lipophilic, MXN alone from liposomal MXN could be transferred to cell membrane. D-FITC is fluorescent, is very hydrophilic and is unable to penetrate cells except via liposome endocytosis as shown in Figure 3. Liposomal DXR was leaky as shown in Figure 2B so that cellular uptake could not be investigated.

As for the influence of the lipid composition on cellular uptake 2 h after incubation, F/HSPC-L, which has lower lipid membrane fluidity, showed about 2-fold higher association than F/DMPC-L (P < 0.01). Non-folate liposomes were taken up similarly regardless of lipid composition.

Flow cytometry analysis showed a shift in the curve and a clear increase in cellular uptake of F/HSPC-L and F/DMPC-L after 2 h exposure to KB cells (Figure 4A). In addition, the mean fluorescence intensity of F/HSPC-L had 2.9-fold greater association than that of F/DMPC-L. In contrast, non-folate liposomes such as HSPC-L and DMPC-L shifted very little. The rank order of the potential of the liposomes to deliver encapsulated D-FITC into the cells was F/HSPC-L > F/DMPC-L > HSPC-L = DMPC-L. In contrast, the cellular uptake of liposomes into A549 cells was not observed (Figure 4B). The results indicate that folate-targeted liposomes were transported into cells by an FR-mediated endocytosis process. These findings were consistent with a previous report on the FR-mediated cellular uptake of folate-targeted liposomes and emulsions in KB cells.[5,14]

(22) Ugwu, S.; Zhang, A.; Parmar, M.; Miller, B.; Sardone, T.; Peikov, V.; Ahmad, I. Preparation, characterization, and stability of liposome-based formulations of mitoxantrone. *Drug Dev. Ind. Pharm.* **2005**, *31* (2), 223–229.

(23) Anderson, M.; Omri, A. The effect of different lipid components on the in vitro stability and release kinetics of liposome formulations. *Drug Delivery* **2004**, *11* (1), 33–39.

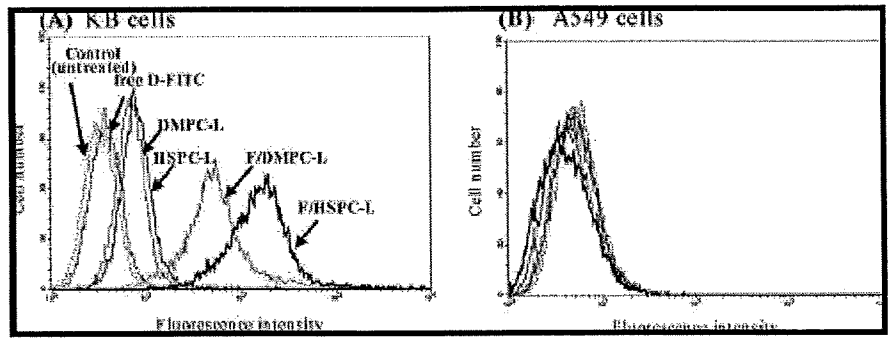

Figure 4. Cellular uptake of liposomes encapsulating D-FITC with KB (A) or A549 (B) cells by flow cytometry after 2 h incubation. Control indicates autofluorescence of untreated cells.

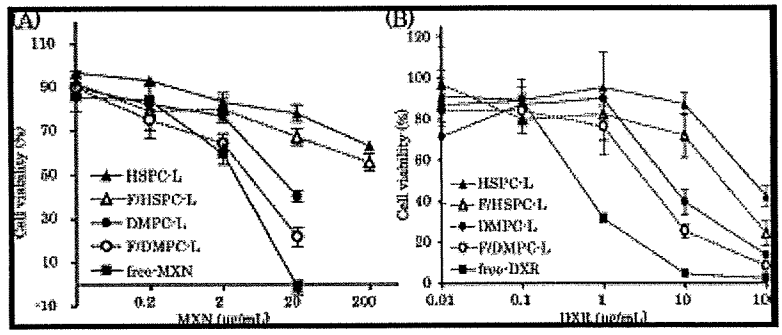

Figure 5. Cytotoxicity of liposomal MXN (A) or DXR (B) against KB cells. Cells were incubated with liposomes in folate-free medium for 2 h, then in fresh medium without the drug for 48 h at 37 °C. Each value represents mean ± SD ($n = 5$).

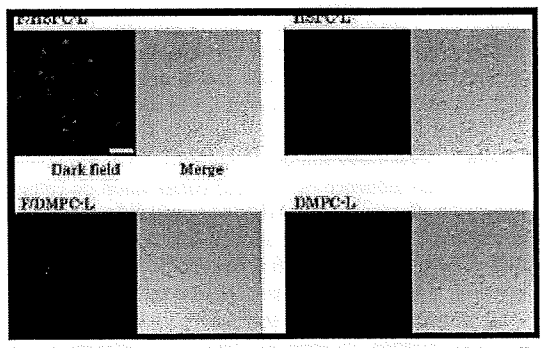

Figure 6. Confocal microscopic images of KB cells treated with liposomes encapsulating D-FITC after 24 h incubation. Scale bar denotes 100 μm (×200).

However, this is the first report that folate-targeted HSPC-L has a much higher uptake rate into FR (+) cells than DMPC-L. FR-mediated liposomes with low liposomal membrane fluidity were taken up more effectively into KB cells, suggesting that an anchor part with lower flexibility might restrict the movement of the hydrated, flexible PEG linker, resulting in high recognition efficiency of the folate ligand by FR.

3.4. Cytotoxicity Study. The cytotoxicity of liposomal MXN or DXR formulations to KB cells was evaluated by a WST-8 assay (Figure 5). Folate-targeted liposomes showed significantly higher cytotoxicity than non-folate-targeted liposomes, which corresponded to their cellular uptake rate. Empty-liposomes into which the drugs were not loaded did not show any toxicity to KB cells (data not shown). However, as for the influence of lipid composition on cytotoxicity, MXN-loaded DMPC-L with higher membrane fluidity showed higher toxicity than HSPC-L. The rank order of cytotoxicity to the cells was HSPC-L < F/HSPC-L < DMPC-L < F/DMPC-L < free-MXN in KB cells (Figure 5A). MXN concentrations leading to 50% cell death (IC_{50}) were determined from concentration-dependent cell viability curves. The IC_{50} values of each liposomal MXN formulation were HSPC-L = F/HSPC-L > 200 μg/mL, DMPC-L = 10.9 μg/mL, F/DMPC-L = 4.3 μg/mL, and free-MXN = 2.9 μg/mL. Surprisingly, this finding was in conflict with the results of the cellular uptake study. Since the release of MXN from all liposomes during incubation with cells was quite low regardless of folate-linkage, cytotoxicity was considered to reflect drug release from the liposomes in the endosomes into the cytoplasm. Therefore, this finding indicates that liposomal membranes with higher fluidity easily released MXN.

Similar to MXN, DXR-loaded DMPC-L with high fluidity showed higher cytotoxicity (Figure 5B), corresponding to the higher release of DXR (Figure 2B). This finding indicated that DXR released from DMPC-L into the extracellular medium mediated the cytotoxic effect. This finding corresponded with the previous report.[15] The IC_{50} values of each liposomal DXR formulation were HSPC-L = 66.8 μg/mL, F/HSPC-L = 28.3 μg/mL, DMPC-L = 3.9 μg/mL, F/DMPC-L = 3.3 μg/mL, and free-DXR = 0.47 μg/mL.

3.5. Cellular Uptake Observed by Confocal Microscopy. To investigate differences in cellular uptake and cytotoxicity of liposomal MXN, the intracellular localization of the various liposome formulations encapsulating D-FITC was observed by confocal microscopy (Figure 6). KB cells were exposed to liposomes for 24 h. Until 24 h, the liposomes were barely detectable because the fluorescence intensity of D-FITC was not particularly strong. The fluorescence of D-FITC in folate-targeted liposomes was observed clearly after 24 h incubation, whereas that of non-folate liposome was weak. In particular, the fluorescence from F/HSPC-L was significant in its extent, which corresponded with the results of cellular uptake and flow cytometry (Figures 3 and 4A).

To compare the cellular uptake of D-FITC with DXR, the intracellular localization of the various liposomal DXR formulations was observed (Figure 1s in the Supporting Information). After incubation for 1, 2, 6, and 24 h, the fluorescence of DXR in folate-targeted liposomes was observed more clearly than with non-folate liposomes. In contrast to D-FITC, DXR in both F/DMPC-L and DMPC-L were taken up into cells much more strongly than F/HSPC-L and HSPC-L. This finding reflected that DXR-loaded F/DMPC-L and DMPC-L were significantly more leaky than F/HSPC-L and HSPC-L (Figure 2B), which corresponded with the findings of the previous report.[24] Furthermore, although leakage of DXR from liposomes contributed to the cytotoxicity of liposomal DXR, the uptake via FR-mediated endocytosis also contributed, since there was no significant difference in release between F/DMPC-L and DMPC-L (Figure 2B), but the former showed higher toxicity than the latter (Figure 5B).

The cellular uptake of F/HSPC-L was higher than F/DMPC-L and non-folate liposomes, suggesting that folate was effectively recognized by FR when the anchor lipid was locked into the liposomes. On the contrary, the uptake of non-folate HSPC- and DMPC-L was similar, even if leakage and/or fusion of the liposomes with the plasma membrane occurred over endocytosis. From this study it can be concluded that, for FR-mediated uptake, liposomal membranes with lower fluidity were more effective. On the contrary, for the release of liposomal drugs from the endosome into the cytoplasm, liposomes with high fluidity were more effective irrespective of the existence of folate modifications. This is one of the reasons why the in vivo antitumor efficacy of liposomal MXN with higher fluidity liposomes was more effective, which was different from DXR. The choice of the appropriate lipid composition for FR-targeting liposomes is important to obtain a formulation that fits all the necessary criteria for each clinical application.

Conclusion

In this study, F/HSPC-L exhibited higher cellular uptake via FR-mediated endocytosis into FR (+) KB cells but lower cytotoxicity than F/DMPC-L. High cytotoxic activity of folate-targeted liposomal MXN was achieved by selecting lipids with higher lipid membrane fluidity though cellular uptake was restricted. This may be a novel finding for the design of liposomes in FR-targeting liposomes in the clinical setting. However, further in vivo evaluation of this new formulation is warranted.

Acknowledgment. This study was supported in part by the Ministry of Education, Culture, Sports, Science and Technology of Japan, and by the Open Research Center Project.

Supporting Information Available: Figure 1s, confocal microscopic images of KB cells incubated with liposomal DXR for 1, 2, 6, and 24 h. This material is available free of charge via the Internet at http://pubs.acs.org.

MP800069C

(24) Kobayashi, T.; Ishida, T.; Okada, Y.; Ise, S.; Harashima, H.; Kiwada, H. Effect of transferrin receptor-targeted liposomal doxorubicin in P-glycoprotein-mediated drug resistant tumor cells. *Int. J. Pharm.* **2007**, *329* (1−2), 94–102.

Combination of RET siRNA and irinotecan inhibited the growth of medullary thyroid carcinoma TT cells and xenografts *via* apoptosis

Kimiko Koga,[1] Yoshiyuki Hattori,[1,3] Mihoko Komori,[1] Ryota Narishima,[2] Masahiro Yamasaki,[2] Motoki Hakoshima,[1] Tetsuya Fukui[2] and Yoshie Maitani[1]

[1]Institute of Medicinal Chemistry, [2]Department of Health Chemistry, Hoshi University, Shinagawa-ku, Tokyo, Japan

(Received October 26, 2009/Revised December 16, 2009/Accepted December 19, 2009)

Medullary thyroid carcinoma (MTC) is a rare endocrine tumor that frequently metastasizes, and treatment with irinotecan (CPT-11) is limited because of side effects. Mutations in the Rearranged during transfection (RET) proto-oncogene are considered the causative event of MTC. The objective of this study was to examine whether small interfering RNA (siRNA) and its combined treatment with CPT-11 could inhibit MTC cell growth *in vitro* and *in vivo*. The transfection of RET siRNA suppressed RET expression, reduced proliferation, and increased caspase-3/7 activity *via* the down-regulation of Bcl-2 expression. Combined treatments with CPT-11 or SN-38 significantly increased caspase 3/7 activity compared with RET siRNA, CPT-11 or SN-38 treatment alone. Importantly, intratumoral injection of RET siRNA along with intravenous injection of CPT-11 significantly inhibited the tumor growth of MTC xenografts *via* an increased apoptotic effect. These findings that RET siRNA enhanced sensitivity for CPT-11 will provide a novel strategy for the treatment of MTC with RET mutation. (*Cancer Sci* 2010)

Medullary thyroid carcinoma (MTC) is a rare endocrine tumor originating from calcitonin-secreting C cells. MTC may be sporadic or hereditary, including multiple endocrine neoplasia (MEN) type 2A, MEN type 2B and familial medullary thyroid carcinoma (FMTC).[1] MTC has an overall 10-year cause-specific survival of 60–70%, with a particularly poor prognosis for patients with MEN2B and sporadic MTC, who have a 5-year mortality of 30–50%.[2] Hereditary MTC is caused by a germline mutation in the Rearranged during transfection (RET) gene. About 40% of sporadic MTCs harbor a somatic RET mutation.[3] The RET gene encodes a receptor tyrosine kinase with an extracellular ligand-binding domain and a cysteine-rich domain, a signal transmembrane domain and an intracellular domain containing the catalytic tyrosine kinase domain.[3] RET has a glial cell line-derived neurotrophic factor as a ligand,[4] but mutated RET leads to a constitutive active RET tyrosine kinase, causing malignant behavior of C cells.[5]

Surgery is currently the only effective treatment for primary MTC.[6] Radioactive iodine has no benefit since C cells do not take up iodine. The role of chemotherapeutic regimens is also limited.[7] Imatinib specifically inhibits the tyrosine kinase activity of Abl, Kit and platelet-derived growth factor receptor (PDGFR).[8] However, imatinib therapy for MTC yielded no objective responses and induced considerable toxicity in patients.[9] CPT-11 injected intraperioneally was relatively effective for TT tumor xenografts.[10] There is, therefore, no curative therapy for patients with metastatic MTC, which is responsible for many of the deaths caused by MTC. Gene therapy is a potentially useful alternative treatment for MTC. Specific inhibition of RET signaling using the dominant-negative RET mutant and ribozyme resulted in both growth suppression and subsequently the death of MTC cells.[11–13] Expressions of thymidine kinase, interleukin (IL-2) and IL-12 by adenoviral vectors have resulted in tumor suppression in MTC animal models;[14] however, the observed antitumor effect *in vivo* was mostly transient.

New technology based on specific inhibition of the RET gene may be useful for MTC treatment to improve safety. RNA interference (RNAi) is a powerful gene-silencing process that holds great promise in the field of cancer therapy.[15] Small interfering RNAs (siRNAs) are expected to have a medicinal application in human gene therapy as drugs with high specificity for molecular targeting. RET siRNA can inhibit the expression of RET tyrosine kinase receptor, and it is expected to inhibit all signals following RET tyrosine kinase; however, gene therapy with RET siRNA has not been reported *in vivo* for thyroid cells endogenously expressing mutated RET.

It is rational to select tyrosine kinase inhibitors for the treatment of MTC, although a selective drug that targets RET has not yet been found. Therefore, in this study, we selected RET siRNA as potentially therapeutic molecules. Human MTC (TT) cells endogenously expressed RET bearing the C634W mutation associated with MEN2A mutations, which have been identified mainly in one of six cysteine residues (codon 609, 611, 618, 620 in exon 10, and codon 630, 634 in exon 11) in the RET extracellular domain;[6,16] therefore, TT cells are useful as a model for studying MTC.[16]

In this study, we investigated whether the transfection of RET siRNA alone and in combination with CPT-11 could induce the growth inhibition of TT cells and tumor xenografts. Combination therapy with RET siRNA and CPT-11 may be effective for MTC.

Materials and Methods

Cell culture. TT cells were obtained from the European Collection of Cell Cultures (ECACC, Wiltshire, UK). The cells were grown in Ham's F-12 culture medium (Wako, Osaka, Japan) supplemented with 10% heat-inactivated fetal bovine serum (FBS) (Gibco BRL) at 37°C in a 5% CO_2 humidified atmosphere.

siRNA. The stealth RNA interference duplex-targeting nucleotides of RET (RET-1 siRNA, RET 2-siRNA and RET-3 siRNA) and stealth RNAi Negative Control Low GC Duplex and Medium GC Duplex as control siRNAs (Cont-L siRNA and Cont-M siRNA, respectively) were synthesized by Invitrogen (Carlsbad, CA, USA). The stealth siRNA sequences of RET were RET-1 sense: 5′-AAAUCCGAAAUCUUCAUCUUCCGCC-3′ and antisense strand 5′-GGCGGAAGAUGAAGAUUUCGGAUUU-3′, RET-2: sense 5′-AAUCCUCUUCAUAAACAUCUCGGGA-3′ and antisense 5′-UCCCGAGAUGUUUAU-

[3]To whom correspondence should be addressed. E-mail: yhattori@hoshi.ac.jp

doi: 10.1111/j.1349-7006.2010.01484.x

GAAGAGGAUU-3′, RET-3: sense 5′-AAAUCAGGGAGUCAGAUGGAGUGGA-3′ and antisense 5′-UCCACUCCAUCUGACUCCCUGAUUU-3′. RET siRNA cocktail is used as a cocktail of three duplexes (100 nmol of RET stealth siRNA cocktail containing 33.3 nmol of each individual siRNA).

Western blotting. TT cells were transfected at a concentration of 100 nM siRNA by Lipofectamine 2000 (Invitrogen Corp.), and then incubated for 72 h. Cell protein extracts were prepared with sampling buffer containing 1% Triton X-100 in phosphate-buffered saline pH 7.4 (PBS), and then Western blotting was performed as previously reported.[17] Expression of RET protein was identified using rabbit anti-RET polyclonal antibody (Santa Cruz Biotechnology, Inc., Santa Cruz, CA, USA) and goat anti-rabbit IgG peroxidase conjugate (Santa Cruz Biotechnology) as the secondary antibody. Expression of Bcl-2 and β-actin protein was identified as previously described.[17]

Antiproliferative activity. TT cells at 50% confluence in 96-well plates were transfected with 100 nM siRNA by Lipofectamine 2000, and then incubated for 72 h. In combination with CPT-11 or SN-38, the culture medium was exchanged for medium containing CPT-11 (Irinotecan; Yakunuto, Tokyo, Japan) ranging from 0.1 to 1000 μg/mL or SN-38 (ethyl-10-hydroxy-camptothecin; Wako, Osaka, Japan) ranging from 0.001 to 10 μg/mL 48 h after transfection of siRNA, and then incubated for another 48 h. After incubation, cell viability was measured by a cell proliferation assay kit (Dojindo, Kumamoto, Japan) as previously reported.[17]

The numbers of dead cells after treatment with RET siRNA, CPT-11, SN-38 or their combination were measured by propidium iodide (PI) staining. The cells were transfected with 100 nM siRNA and then incubated for 48 h. The culture medium was exchanged for medium containing 10 μg/mL CPT-11 or 0.2 μg/mL SN-38, and then incubated for another 48 h. The percentage of PI-positive cells was determined by examining fluorescence intensity on a FACSCalibur flow cytometer (Becton Dickinson, San Jose, CA, USA) as previously described.[17]

Real-time RT-PCR for quantification of RET and Bcl-2 mRNA. TT cells at 50% confluence in 6-well plates were transfected with 100 nM siRNA with Lipofectamine 2000 and then incubated for 72 h. Total RNA was isolated from transfected cells using the NucleoSpin RNA II (Macherey-Nagel, Dueren, Germany). SYBR green quantitative RT-PCR amplification for Bcl-2 and β-actin cDNA was carried out by MyiQ™ Single Color Real-Time PCR Detection System (Bio-Rad Laboratories, Hercules, CA, USA) as previously reported.[17] For the amplification of human RET cDNA, primers RET-FW, 5′-GGCAGCCAGAAACATCCT-3′, and RET-RW, 5′-ACTTTGCGTGGTGTAGAT-3′, were used.

Caspase 3/7 assay. TT cells at 50% confluence in 12-well plates were transfected with 100 nM siRNA using Lipofectamine 2000 and then incubated for 48 h. The culture medium was then exchanged for medium containing 10 μg/mL CPT-11 or 0.2 μg/mL SN-38 and then incubated for another 48 h. After the incubation, caspase 3/7 activity was measured by Caspase3/7 assay system (Caspase-Glo® 3/7 assay; Promega, Madison, WI, USA) as previously reported.[18]

Assessment of TT tumor growth. Female ICR nu/nu mice (6 weeks of age) were purchased from Oriental Yeast Co., Ltd. (Tokyo, Japan). To generate TT tumor xenografts, 1×10^7 TT cells suspended in 50 μL PBS containing 50% Matrigel (Collaborative Research, Bedford, MA, USA) were inoculated subcutaneously into the flank region of mice. When the average volume of xenograft tumors reached about 100 mm^3, therapy was started (day 0). For siRNA transfection *in vivo*, we used cationic nanoparticles (NP) consisting of cholesteryl-3β-carboxyamidoethylene-*N*-hydroxyethylamine as a cationic lipid, and 5 mol% Tween-80, as previously reported.[19] For transfection into tumors, 10 μg siRNA was mixed with NP at a charge ratio (+/−) of cationic lipid/siRNA of 1/1 with gentle shaking and standing for 15 min at room temperature. The complex of NP and siRNA was directly injected into the xenografts on days 0, 3, and 6, and CPT-11 was intravenously injected at a dose of 30 mg/kg on day 2, 5, and 8. On 24 days, blood was collected into tubes and centrifuged to separate plasma from blood cells. Serum concentrations of calcitonin were measured using a human calcitonin ELISA kit (Biosource International, Inc., CA, USA). Animal experiments were conducted with ethics approval from our institutional animal care and use committee.

Preparation of probes for *in situ* hybridization. The RET cDNA fragment (873 bp) was amplified from TT cells cDNA. The RET primers used for RET cDNA amplification were: forward primer, 5′-TCCTGGGAGAAGCTCAGTGT-3′ and reverse primer, 5′-CACGTTGAAGTGGAGCAAGA-3′. The fragments were cloned into pGEM-T vector (Promega), and ^{35}S-labeled cRNA probes were prepared as previously reported.[20]

***In situ* hybridization.** For transfection into tumors, the complex of NP and 10 μg siRNA per tumor was directly injected into TT tumor xenografts on days 0, 3, and 6. At 48 h after final injection the tumors were frozen in powdered dry ice, and

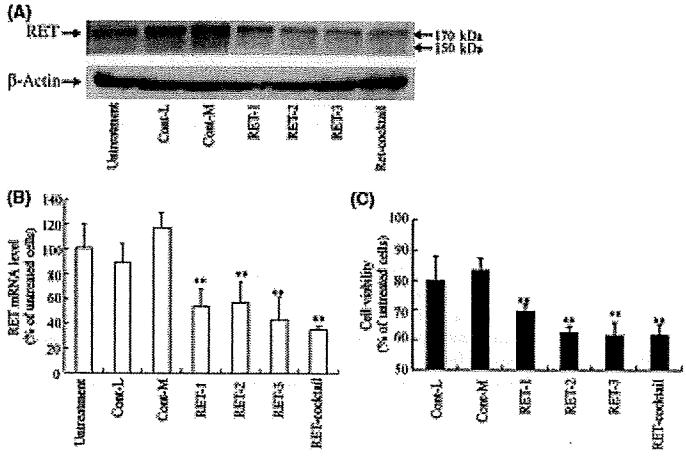

Fig. 1. Inhibition of RET expression by transfection of RET siRNA with Lipofectamine 2000 into TT cells. Expressions of RET protein (170 KDa) and mRNA were detected by Western blot (A) and quantitative RT-PCR (B) analyses, respectively, 72 h after transfection with 100 nM Cont-L and -M siRNA, RET-1, -2 and -3 siRNA and their cocktail. The number of viable cells was determined by WST-8 assay 72 h after transfection (C). $n = 4$ for each sample. $^{**}P < 0.01$, compared with Cont-L siRNA transfected cells.

doi: 10.1111/j.1349-7006.2010.01484.x

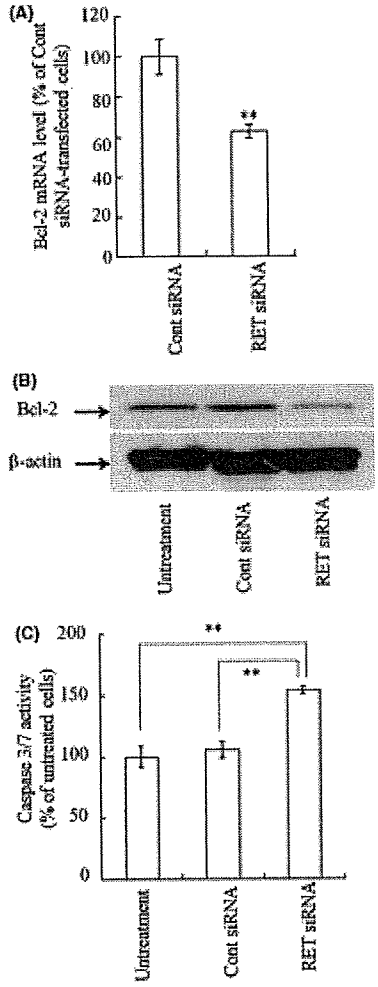

Fig. 2. Effect of transfection with RET siRNA with Lipofectamine 2000 on Bcl-2 expression and caspase 3/7 activity in TT cells. Cells were incubated for 72 h after transfection with 100 nM RET siRNA or Cont siRNA. Expressions of Bcl-2 mRNA and protein were detected by quantitative RT-PCR (A) and Western blot (B). Caspase 3/7 activity was measured by caspase 3/7 luminometric assay (C). $n = 4$ for each sample. $^{**}P < 0.01$.

coronal sections were cut 16 μm thick with a cryostat, thaw-mounted onto gelatin and poly-lysine-coated slides. *In situ* hybridization was carried out as previously described.[20] All sections were counterstained with hematoxylin and eosin.

***In vivo* detection of apoptosis.** For siRNA transfection into tumors, 10 μg siRNA per tumor was directly injected by NP into TT tumor xenografts on days 0, 3, and 6. CPT-11 was intravenously injected at a dose of 30 mg/kg on day 2, 5, and 8. On day 11, the Red *in vivo* FLIVO™ apoptosis Kit (Immunochemistry Technologies, Bloomington, MN, USA) was injected *i.v.* and allowed to circulate for 30 min. The tumors were frozen in powdered dry ice, and coronal sections were cut 20 μm thick with a cryostat, thaw-mounted onto poly-lysine-coated slides. The specimens were examined microscopically using an Eclipse TS100-F microscope (Nikon, Tokyo, Japan).

Statistical analysis. The statistical significance of the data was evaluated with Student's *t*-test. $P < 0.05$ was considered significant.

Results

***In vitro* growth inhibitory effect of RET siRNA.** We initially characterized the expression of RET protein in TT cells after transfection of RET siRNA with Lipofectamine 2000. Here, we used RET-1, RET-2, RET-3 and their cocktail siRNAs as RET siRNAs (40%, 44%, 48%, and 44% in GC contents of the siRNA sequence, respectively), and Cont-L and -M siRNAs as negative control siRNAs (36% and 48% in GC contents of the siRNA sequence, respectively). Expression of RET protein was strongly suppressed in TT cells 48 h after transfection of RET-1, RET-2, RET-3 siRNA or their siRNA cocktail, but unaffected by the transfection of Cont-L or -M siRNA (Fig. 1A). Furthermore, the transfection of RET siRNA suppressed the expression of RET mRNA to about 40–50% of untransfected cells (Fig. 1B).

To investigate whether the suppression of RET expression induced the inhibition of cell growth, we examined cell viability 72 h after transfection of RET siRNA at 100 nM. After transfection, the cell viabilities of all RET siRNAs were 60–70%, but those of Cont-L and -M were 80 and 83%, respectively (Fig. 1C). When transfected at a concentration of 12.5 nM siRNA, the RET siRNA cocktail showed a stronger decrease of cell viability (67%) than RET-1, RET-2 and RET-3 siRNA (76, 72, and 75%, respectively) (data not shown). The slight inhibition of cell growth by transfection with Cont-L and -M siRNA may be due to the toxicity of Lipofectamine 2000. In subsequent studies, we used the RET siRNA cocktail as a RET siRNA, and Cont-L siRNA as a control siRNA.

Bcl-2 expression and caspase 3/7 activity after transfection with RET siRNA into TT cells. It has been reported that the expression of a dominant-negative RET down-regulated the expression of Bcl-2.[21] Therefore, we investigated whether transfection of RET siRNA affected Bcl-2 expression in TT cells (Fig. 2A,B). Transfection of RET siRNA decreased the expression of Bcl-2 mRNA and protein (Fig. 2A,B) and furthermore, significantly increased caspase 3/7 activity in cells compared with Cont siRNA (Fig. 2C). These findings suggested that the suppression of RET expression may increase caspase 3/7 activity *via* the down-regulation of Bcl-2 expression.

***In vitro* sensitivity of CPT-11 or SN-38.** Here, we used CPT-11 as a potent antitumor drug for TT tumor xenografts, because it has been reported that MTC cell lines were sensitive to a topoisomerase I inhibitor, camptothecin (CPT).[22] To investigate whether the transfection of RET siRNA enhanced sensitivity for chemotherapy, we incubated CPT-11 or its active metabolite SN-38 for 48 h in the cells 48 h after transfection of RET siRNA. In cells transfected with RET siRNA, cytotoxicities by CPT-11 and SN-38 were similar with those in cells transfected with Cont siRNA (Fig. 3A,B), indicating that their activities were at least additive for tumor suppression by RET siRNA.

We next investigated whether RET siRNA transfection affected the number of cell deaths and caspase 3/7 activity by CPT-11 or SN-38 treatment. The cells were transfected with RET or Cont siRNA for 48 h, and then treated with 10 μg/mL CPT-11 or 0.2 μg/mL SN-38 for 48 h, the concentrations of which were around the IC_{50} of CPT-11 and SN-38 in untransfected cells, respectively. To measure the number of cell deaths, PI staining of the cellular nucleus was used as a marker. RET siRNA transfection increased the number of PI-staining cells and caspase 3/7 activity compared with Cont siRNA

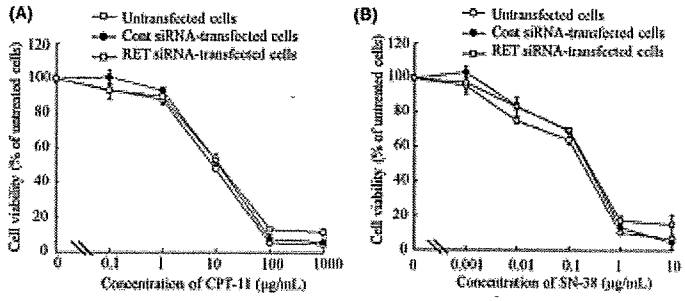

Fig. 3. Concentration-dependent effect of CPT-11 or SN-38 on cytotoxicity after transfection with RET siRNA. Cells were transfected with 100 nM RET siRNA or Cont siRNA with Lipofectamine 2000 and incubated for 48 h. After incubation, the cells were treated with various concentrations of CPT-11 (A) or SN-38 (B) and incubated for another 48 h. The number of viable cells was determined by WST-8 assay. $n = 4$ for each sample.

transfection (Fig. 4A,B). Among treatments, the combination of RET siRNA plus SN-38 significantly increased activity and cells compared to RET siRNA or SN-38 alone (Fig. 4A,B) ($P < 0.01$).

Suppression of RET expression in TT tumor xenografts. Next, we investigated whether the expression of RET mRNA was decreased by intratumoral injection of RET siRNA. Here, we used NP as a siRNA transfection vector for *in vivo* experiments.[19] Cont or RET siRNA was directly injected with NP into TT tumor xenografts 3 times at 3-day intervals and then tumors were excised 2 days after the final injection. The sense probe for the RET gene was used as a negative control probe. Silver grain distribution in the dark field and black grain in the bright field following *in situ* hybridization exhibiting RET mRNA expression (Fig. 5A,B, supplemental Figs S1 and S2). Positive cells for RET mRNA were strongly detected in the tumor cells, but not stroma cells with the antisense probe for the RET gene (Fig. 5B). Most of the tumor cells were positive for the expression of RET mRNA in saline-injected and Cont siRNA-transfected cells. In contrast, RET siRNA transfection decreased the number of silver grains in the dark field (Fig. 5A) and black grains in the bright field (Fig. 5B) in some tumor sections, indicated that the expression of RET mRNA was suppressed by RET siRNA injection.

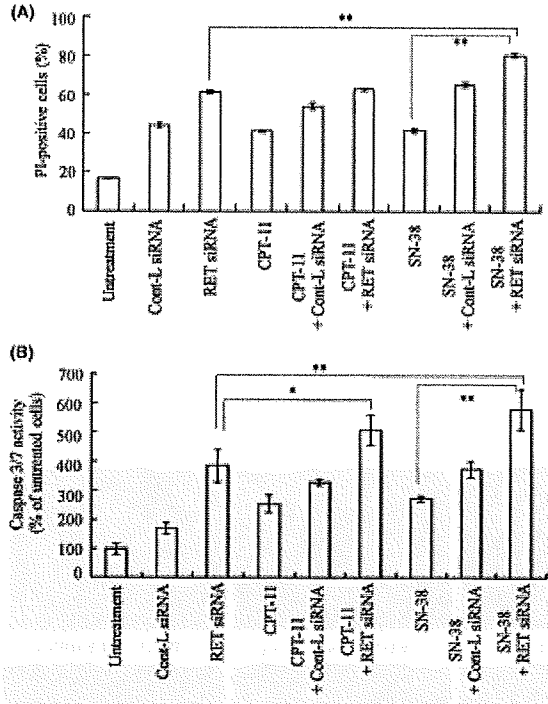

Fig. 4. Dead cells (A) and caspase-3/7 activity (B) by combined treatment with RET siRNA plus CPT-11 or SN-38 in TT cells. The number of dead cells was measured by a FACSCalibur flow cytometer after staining with PI (A). Caspase-3/7 activity was measured by caspase-3/7 luminometric assay (B). $n = 3$ for each sample. *$P < 0.05$, **$P < 0.01$; compared with RET siRNA transfected cells.

Synergistic inhibition of the growth of TT tumor xenografts. We evaluated the efficacy of combination therapy of RET siRNA and CPT-11 in inhibiting the growth of subcutaneous TT tumors. The anti-tumor effect was evaluated by direct injection of Cont or RET siRNA with NP into xenografts once a day three times (day 0, 3, and 6) following three *i.v.* injections of CPT-11 (day 2, 5, and 8). No significant growth inhibitory effect was observed in mice treated with RET siRNA, CPT-11 or CPT-11 plus Cont siRNA compared with mice injected with saline (Fig. 6A). CPT-11 plus Cont siRNA exhibited a similar tumor suppressive effect with CPT-11 alone. A significant growth inhibitory effect was observed in combination therapy with CPT-11 and RET siRNA compared with CPT-11 alone. All treatments, the transfection of RET siRNA, the injection of CPT-11 alone, and their combination did not significantly change body weight during 3 weeks of treatment (data not shown). In this study, the effect of the combination on tumor growth was significantly higher than that of CPT-11 alone at lower doses that did not exhibit serve adverse effects.

RET siRNA transfection alone could not significantly suppress tumor growth. The results of *in situ* hybridization showed that the suppression of RET expression in the tumors was restricted to the tumor in the vicinity of the injection site (data not shown). Strong inhibition of *in vivo* tumor growth by RET siRNA depends on the development of a gene vector having the ability to introduce siRNA widely into tumors.

Serum calcitonin concentration and *In vivo* apoptosis. C cells of the thyroid gland secrete calcitonin, the level of which is elevated in patients with C cell hyperplasia and MTC; therefore, calcitonin is a very sensitive and reliable marker for the presence of MTC, and the level of calcitonin correlates with tumor burden and the response to therapy.[23,24] On day 24 in Fig. 6A, all mice were sacrificed, and serum calcitonin concentration was measured. Serum calcitonin level in TT tumor xenografts showed a 21-fold increase compared with that in normal mice (Fig. 6B). RET siRNA or CPT-11 alone decreased serum calcitonin levels to 39% and 80% compared with saline (Fig. 6B). Corresponding to the highest growth inhibition, the combination of CPT-11 plus RET siRNA markedly decreased the serum calcitonin level to 30%.

To confirm the effectiveness *in vivo*, we detected apoptotic cells 48 h after combination therapy with RET siRNA and

doi: 10.1111/j.1349-7006.2010.01484.x

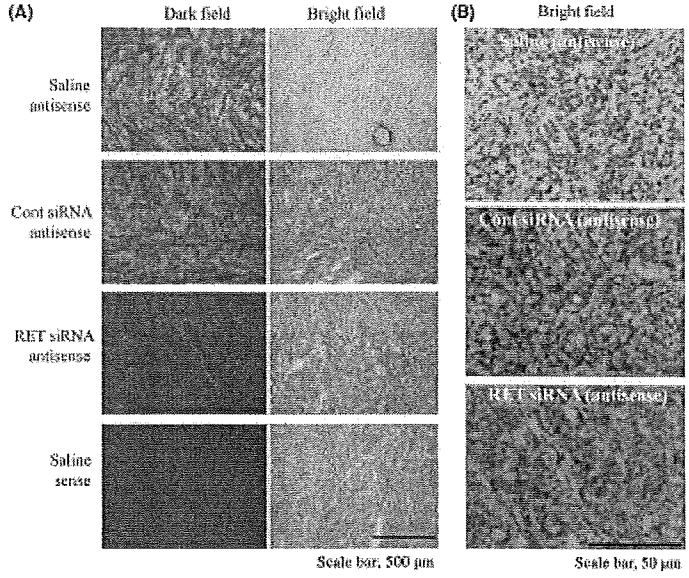

Fig. 5. *In situ* hybridization of a ^{35}S-labeled antisense or sense probe generated against RET mRNA. An antisense probe was used to detect RET mRNA. The sense probe for the RET gene was used as a negative control probe. In (A), silver grains in a dark field indicate RET mRNA expression. Scale bar: 500 μm. In (B), microautoradiographs in bright fields in Fig. 5(A) were enlarged. Black grains indicate RET mRNA expression. Red arrows indicate stroma cells. Scale bar: 50 μm.

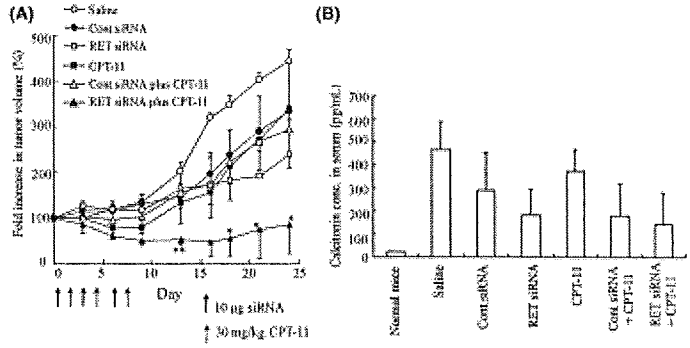

Fig. 6. *In vivo* combination therapy of RET siRNA and CPT-11 for TT tumor xenografts. Ten microgram of RET or Cont siRNA per tumor was directly injected with NP into the tumor on days 0, 3, and 6. CPT-11 at a dose of 30 mg/kg was injected *i.v.* on days 2, 5, and 8. Tumor volume was measured for 24 days (A). $^{*}P < 0.05$, $^{**}P < 0.01$; compared with the group injected with CPT-11. All mice were sacrificed on day 24 and the concentration of calcitonin in blood was measured (B). Data in A and B are shown as the mean ± SE. $n = 3$ for each group.

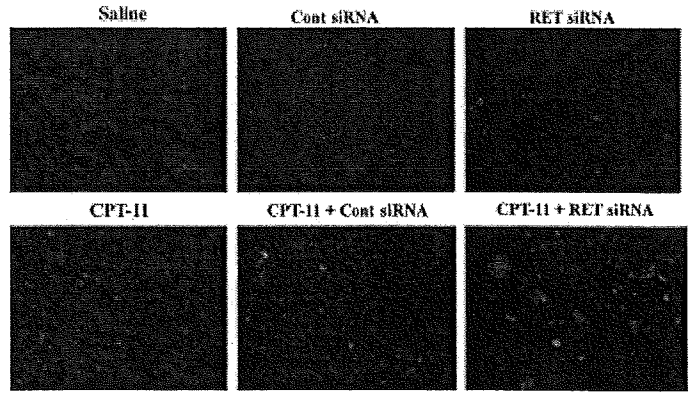

Fig. 7. Distribution of apoptotic cells in TT tumor xenografts after injection of RET siRNA and CPT-11. Experimental conditions were the same as in Fig 6. On day 11, all mice were sacrificed and apoptosis cells were detected by the Red *in vivo* FLIVO™ apoptosis Kit. Red signals indicate apoptotic cells. Magnification ×100.

CPT-11. In tumor sections after injections of RET siRNA or CPT-11 alone, red, indicating apoptotic cells, was slightly observed, but not in saline or Cont siRNA (Fig. 7). On the other hand, combination treatment with RET siRNA plus CPT-11 strongly induced apoptotic cells. These data also indicated that combination therapy was effective for MTC.

Discussion

In this study, we demonstrated that the combination with RET siRNA and CPT-11 could induce the growth inhibition of TT cells and tumor xenografts. Recently, RET siRNA delivered by chitosan-coated poly(isobutylcyanoacrylate) nanoparticles led to tumor growth inhibition after intratumoral administration in mice transplanted with NIH3T3 cells transformed with the ret/PTC1 gene;[25] however, it has been reported that the ret/PTC-1 signaling pathway was different between thyroid and fibroblast cells;[26] therefore, this is the first report that RET siRNA transfected with NP inhibited tumor growth in mice bearing TT cells.

The combination therapy *in vivo* revealed greater than additive effects in cytotoxicity *in vitro*. CPT-11 is known as an effective inhibitor of angiogenesis for endothelial cells in tumor as well as cytotoxic drug.[27] The mechanism of increasing growth inhibition for TT tumor xenografts by RET siRNA and CPT-11 was not clear, although inhibition of receptor tyrosine kinase in tumor cells could sensitize cells to CPT-11.[28,29] Overexpression of Bcl-2 has been observed in MTC,[30,31] and is associated with the poor response of MTC to chemotherapy. The expression of dominant-negative RET in TT cells decreased the expression of Bcl-2 and could reduce cell viability,[21] and the antitumor effect by CPT-11 was enhanced by the combination with RET inhibitor, CEP-751, for TT tumor xenografts.[10] As another possibility, RET has been shown to activate nuclear factor κB (NFκB) *via* the phosphatidylinositol-3-kinase/Akt pathway.[1] Akt mediates multiple cellular responses, such as survival signaling by NFκB activation and BAD inactivation, and cell cycle progression; therefore, inhibition of RET expression might modulate cellular sensitivity through the survival signaling pathway.[32,33] From these findings, the combination of RET siRNA and CPT-11 will have great potential for gene therapy in MTC.

In conclusion, we demonstrated that combining RET siRNA with CPT-11 resulted in significant greater growth suppression of TT cells and tumor xenografts *via* increased apoptosis. As the thyroid gland is anatomically accessible, future treatment of primary MTC tumors by direct intratumoral injection of siRNA/NP complex expressing mutated genes is possible. Thus, the combination of RET siRNA and CPT-11 may serve as a novel tool for gene therapy.

Acknowledgments

We thank Ms. Manami Kubo for assistance with the experimental work. This study was supported in part by the Japan Health Sciences Foundation, by the Ministry of Education, Culture, Sports, Science and Technology of Japan, and by the Open Research Center Project.

References

1 Kodama Y, Asai N, Kawai K *et al.* The RET proto-oncogene: a molecular therapeutic target in thyroid cancer. *Cancer Sci* 2005; **96**: 143–8.
2 Moley JF. Medullary thyroid carcinoma. *Curr Treat Options Oncol* 2003; **4**: 339–47.
3 Hansford JR, Mulligan LM. Multiple endocrine neoplasia type 2 and RET: from neoplasia to neurogenesis. *J Med Genet* 2000; **37**: 817–27.
4 Treanor JJ, Goodman L, de SF *et al.* Characterization of a multicomponent receptor for GDNF. *Nature* 1996; **382**: 80–3.
5 Santoro M, Melillo RM, Carlomagno F, Vecchio G, Fusco A. Minireview: RET: normal and abnormal functions. *Endocrinology* 2004; **145**: 5448–51.
6 Cohen MS, Moley JF. Surgical treatment of medullary thyroid carcinoma. *J Intern Med* 2003; **253**: 616–26.
7 Gimm O. Thyroid cancer. *Cancer Lett* 2001; **163**: 143–56.
8 Jones RL, Judson IR. The development and application of imatinib. *Expert Opin Drug Saf* 2005; **4**: 183–91.
9 de Groot JW, Zonnenberg BA, van Ufford-Mannesse PQ *et al.* A phase II trial of imatinib therapy for metastatic medullary thyroid carcinoma. *J Clin Endocrinol Metab* 2007; **92**: 3466–9.
10 Strock CJ, Park JI, Rosen DM *et al.* Activity of irinotecan and the tyrosine kinase inhibitor CEP-751 in medullary thyroid cancer. *J Clin Endocrinol Metab* 2006; **91**: 79–84.
11 Drosten M, Frilling A, Stiewe T, Putzer BM. A new therapeutic approach in medullary thyroid cancer treatment: inhibition of oncogenic RET signaling by adenoviral vector-mediated expression of a dominant-negative RET mutant. *Surgery* 2002; **132**: 991–7.
12 Drosten M, Stiewe T, Putzer BM. Antitumor capacity of a dominant-negative RET proto-oncogene mutant in a medullary thyroid carcinoma model. *Hum Gene Ther* 2003; **14**: 971–82.
13 Parthasarathy R, Cote GJ, Gagel RF. Hammerhead ribozyme-mediated inactivation of mutant RET in medullary thyroid carcinoma. *Cancer Res* 1999; **59**: 3911–4.
14 Messina M, Robinson BG. Technology insight: gene therapy and its potential role in the treatment of medullary thyroid carcinoma. *Nat Clin Pract Endocrinol Metab* 2007; **3**: 290–301.
15 Pai SI, Lin YY, Macaes B, Meneshian A, Hung CF, Wu TC. Prospects of RNA interference therapy for cancer. *Gene Ther* 2006; **13**: 464–77.
16 Marsh DJ, Theodosopoulos G, Martin-Schulte K *et al.* Genome-wide copy number imbalances identified in familial and sporadic medullary thyroid carcinoma. *J Clin Endocrinol Metab* 2003; **88**: 1866–72.
17 Hattori Y, Yoshizawa T, Koga K, Maitani Y. NaCl induced high cationic hydroxyethylated cholesterol-based nanoparticle-mediated synthetic small interfering RNA transfer into prostate carcinoma PC-3 cells. *Biol Pharm Bull* 2008; **31**: 2294–301.
18 Hattori Y, Fukushima M, Maitani Y. Non-viral delivery of the connexin 43 gene with histone deacetylase inhibitor to human nasopharyngeal tumor cells enhances gene expression and inhibits in vivo tumor growth. *Int J Oncol* 2007; **30**: 1427–39.
19 Yoshizawa T, Hattori Y, Hakoshima M, Koga K, Maitani Y. Folate-linked lipid-based nanoparticles for synthetic siRNA delivery in KB tumor xenografts. *Eur J Pharm Biopharm* 2008; **70**: 718–25.
20 Hattori Y, Koga K, Izumisawa T *et al.* The distribution of mRNA expression and protein after hydrodynamic injection of transgene in mice. *Biol Pharm Bull* 2009; **32**: 755–9.
21 Drosten M, Hilken G, Bockmann M *et al.* Role of MEN2A-derived RET in maintenance and proliferation of medullary thyroid carcinoma. *J Natl Cancer Inst* 2004; **96**: 1231–9.
22 Kaczirek K, Schindl M, Weinhausel A *et al.* Cytotoxic activity of camptothecin and paclitaxel in newly established continuous human medullary thyroid carcinoma cell lines. *J Clin Endocrinol Metab* 2004; **89**: 2397–401.
23 Moley JF, Wells SA, Dilley WG, Tisell LE. Reoperation for recurrent or persistent medullary thyroid cancer. *Surgery* 1993; **114**: 1090–5.
24 Tisell LE, Dilley WG, Wells SA Jr. Progression of postoperative residual medullary thyroid carcinoma as monitored by plasma calcitonin levels. *Surgery* 1996; **119**: 34–9.
25 de Mil H, Bertrand JR, Fusco A *et al.* siRNA nanoformulation against the ret/PTC1 junction oncogene is efficient in an in vivo model of papillary thyroid carcinoma. *Nucleic Acids Res* 2008; **36**: e2.
26 Barone MV, Sepe L, Melillo RM *et al.* RET/PTC1 oncogene signaling in PC Cl 3 thyroid cells requires the small GTP-binding protein Rho. *Oncogene* 2001; **20**: 6973–82.
27 Ji Y, Hayashi K, Amoh Y *et al.* The camptothecin derivative CPT-11 inhibits angiogenesis in a dual-color imageable orthotopic metastatic nude mouse model of human colon cancer. *Anticancer Res* 2007; **27**: 713–8.
28 Koizumi F, Kamzawa F, Ueda Y *et al.* Synergistic interaction between the EGFR tyrosine kinase inhibitor gefitinib ('Iressa") and the DNA topoisomerase I inhibitor CPT-11 (irinotecan) in human colorectal cancer cells. *Int J Cancer* 2004; **108**: 464–72.
29 Shao RG, Cao CX, Shimizu T, O'Connor PM, Kohn KW, Pommier Y. Abrogation of an S-phase checkpoint and potentiation of camptothecin cytotoxicity by 7-hydroxystaurosporine (UCN-01) in human cancer cell lines, possibly influenced by p53 function. *Cancer Res* 1997; **57**: 4029–35.
30 Wang HG, Reed JC. Mechanisms of Bcl-2 protein function. *Histol Histopathol* 1998; **13**: 521–30.

doi: 10.1111/j.1349-7006.2010.01484.x